Photosynth Res (2008) 97:33–53
DOI 10.1007/s11120-008-9306-1

REVIEW

Investigating the mechanisms of photosynthetic proteins using continuum electrostatics

G. Matthias Ullmann · Edda Kloppmann · Timm Essigke · Eva-Maria Krammer · Astrid R. Klingen · Torsten Becker · Elisa Bombarda

Received: 1 February 2007 / Accepted: 10 April 2008 / Published online: 14 May 2008

Abstract Computational methods based on continuum electrostatics are widely used in theoretical biochemistry to analyze the function of proteins. Continuum electrostatic methods in combination with quantum chemical and molecular mechanical methods can help to analyze even very complex biochemical systems. In this article, applications of these methods to proteins involved in photosynthesis are reviewed. After giving a short introduction to the basic concepts of the continuum electrostatic model based on the Poisson–Boltzmann equation, we describe the application of this approach to the docking of electron transfer proteins, to the comparison of isofunctional proteins, to the tuning of absorption spectra, to the analysis of the coupling of electron and proton transfer, to the analysis of the effect of membrane potentials on the energetics of membrane proteins, and to the kinetics of charge transfer reactions. Simulations as those reviewed in this article help to analyze molecular mechanisms on the basis of the structure of the protein, guide new experiments, and provide a better and deeper understanding of protein functions.

Keywords Poisson–Boltzmann equation · Electrostatic potential · Membrane potential · Master equation · Docking · Spectral tuning · pH and redox titration

G. M. Ullmann (✉) · E. Kloppmann · T. Essigke · E.-M. Krammer · A. R. Klingen · T. Becker · E. Bombarda (✉)
Structural Biology/Bioinformatics, University of Bayreuth, Universitätsstr. 30, BGI, Bayreuth 95447, Germany
e-mail: Matthias.Ullmann@uni-bayreuth.de

E. Bombarda
e-mail: Elisa.Bombarda@uni-bayreuth.de

Introduction

Models play a major role in science. Not only theoretical calculations take advantage of models, but also the interpretation of experimental data relies on models of the system under study. A model is a generalized hypothetical description which gives a simplified representation of a real system intended to enhance our ability to understand, predict, and control its behavior. When a model is made, there are always approximations involved. Therefore a model is always an idealized representation of the real system. A model should be able to explain experimental data and make predictions about the outcome of new experiments. In order to be able to make predictions, a model has to represent all the important aspects of the real system at an appropriate level of description. However, the more complicated and complex a model is, the more difficult it becomes to interpret the results obtained from the model. Therefore, in order to optimally promote our understanding of the real system, the model should be only as complicated as necessary and not more complicated.

When biomolecular systems are modeled, two different aspects need to be considered: the dimension of the system and, if information about the dynamics is desired, the time span over which the system should be modeled. The methods to model biomolecular systems can be classified into the following categories: quantum mechanics, molecular mechanics, and continuum electrostatics (Fig. 1). The methods based on quantum mechanics allow to model molecules at the electronic level (Jensen 1999). With these methods, all electronic degrees of freedom are considered explicitly. Thus, it is possible to treat processes like chemical reactions which involve bond breaking and formation as well as excited state processes. However, quantum mechanical methods are normally restricted to

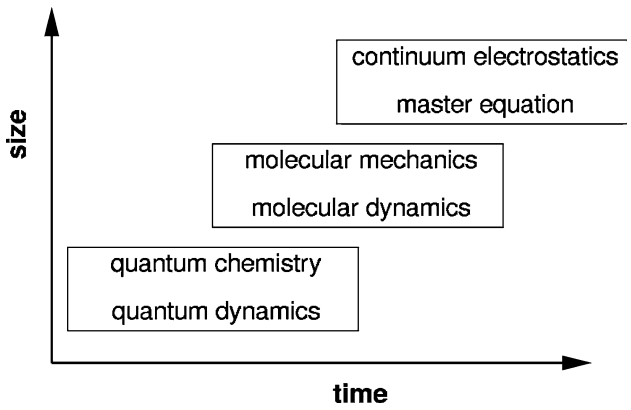

Fig. 1 Theoretical methods applied to model biomolecular systems. Several methods exist to model biomolecular systems. Depending on the level of detail that is required in the simulation, the size of the systems that should be simulated, and the time span over which the system needs to be analyzed, different approaches have to be chosen. A combination of different approaches allows also to combine the advantages of the different methods

relatively small systems and very short time spans. Usually, only the active sites of proteins can be treated by these methods. If the dynamics of whole proteins need to be considered, molecular mechanics is the approach of choice (van Gunsteren et al. 2001). In molecular mechanics, which relies on Newton's mechanics, electrons and nuclei are considered together in spherical atoms which interact with each other covalently and non-covalently in larger molecular ensembles. The main restriction of molecular mechanics is that it cannot be applied to processes that involve bond breaking or bond formation. Systems of medium size can be simulated over time spans not longer than a few microseconds. Such simulations require an enormous amount of computing time mainly because a large fraction of this computing time is needed to simulate the water solvating the protein. For this reason, molecular mechanics cannot be applied when information about longer time scales or many different states of a molecule are required. If calculations of the energetics of many different states are required, continuum electrostatics, which relies on Maxwell's equations, is the approach of choice (Honig and Nicholls 1995). In continuum electrostatics, the protein and the surrounding solvent are described as dielectric continua. In this framework, properties of biomolecules based on electrostatic interactions can be well described. Since electrostatic interactions play a major role in biomolecular systems, continuum electrostatics has a broad range of applications in biomolecular modeling. In combination with a master equation approach, continuum electrostatics can even be used to describe the reaction kinetics of complex systems. All these different types of approaches can be combined. For instance, the active site of an enzyme can be described quantum chemically, the protein surrounding that does not undergo chemical transitions can be described by molecular mechanics and the solvent can be treated as a dielectric continuum (Luo et al. 2002; Prabhu et al. 2004; Senn and Thiel 2007; Friesner and Beachy 1998; Leach 1996).

In this article, we will review applications of continuum electrostatic methods to analyze the function of photosynthetic proteins. In the beginning of this article, the electrostatic model based on the Poisson–Boltzmann equation is described. Afterward, we discuss how this model was used to analyze the association of biomolecules, the tuning of absorption spectra of pigment complexes, the thermodynamics of the coupling of proton and electron binding, the influence of membrane potential and pH gradient on the protonation behavior of membrane proteins, and finally we also describe the application of this model to simulate the electron transfer dynamics in proteins.

The continuum electrostatic model based on the Poisson–Boltzmann equation

The basic idea of the continuum electrostatic approach is relatively simple (Fig. 2). The protein is assumed to have a fixed structure and is modeled as a low dielectric region which is embedded in a high dielectric region representing the solvent. The atoms of the protein are considered as spatially fixed point charges. These point charges allow to represent charged amino acids in the protein such as aspartate and glutamate residues but also dipoles, for instance of the protein backbone or of the side chains of uncharged amino acids. The low dielectric region of the

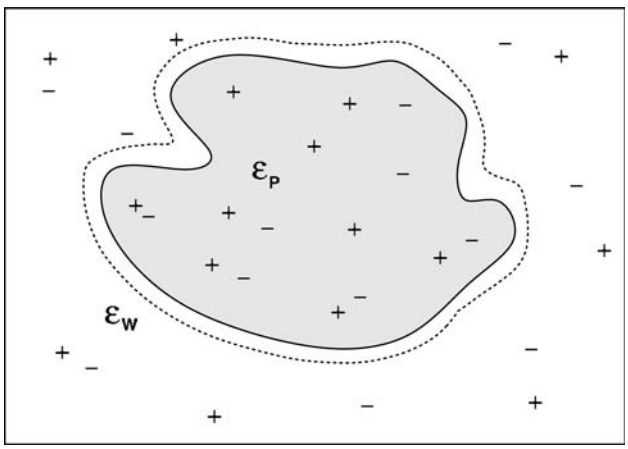

Fig. 2 Conceptual model of the continuum electrostatic approach. The protein (gray) is modeled as a dielectric continuum of low permittivity ε_p with fixed point charges embedded in an environment with a high dielectric permittivity ε_w representing the solvent. The dashed line marks the so-called Stern layer or ion-exclusion layer. In the continuum with a high permittivity, a charge density represents the ions dissolved in the aqueous solution

protein is defined by assigning an atomic radius to all atoms and determining the solvent excluded volume by rolling a sphere over the protein (Richards 1977). Ions that can be dissolved in the solvent are represented by a charge density that adopts a Boltzmann distribution in the solution, but the ions are excluded from entering the protein.

This conceptual model can be translated into a mathematical model in the form of the linearized Poisson–Boltzmann equation (Hill 1960; Ullmann and Knapp 1999; Gunner and Alexov 2000)

$$\nabla[\varepsilon(\mathbf{r})\nabla\phi(\mathbf{r})] = -\rho_f(\mathbf{r}) + \varepsilon(\mathbf{r})\bar{\kappa}^2(\mathbf{r})\phi(\mathbf{r}) \quad (1)$$

where $\varepsilon(\mathbf{r})$ is the permittivity of the medium which varies spatially (inside and outside of the protein), ∇ is the differential operator, $\phi(\mathbf{r})$ is the electrostatic potential, $\rho_f(\mathbf{r})$ is the charge distribution within the protein, and $\bar{\kappa}^2(\mathbf{r})$ is the modified Debye–Hückel parameter which represents a screening factor related to the charge distribution within the aqueous solution.

An analytical solution of this partial differential equation can be obtained only for special geometries such as charged spheres, infinitely long charged cylinders, and charged surfaces. For most other cases, the Poisson–Boltzmann equation needs to be solved numerically. Usually, finite difference methods are used to solve the Poisson–Boltzmann equation. Several computer programs exist to solve the Poisson–Boltzmann equation numerically; among them are MEAD (Bashford 1997), DELPHI (Honig and Nicholls 1995), APBS (Baker et al. 2001), and the PBEQ module of CHARMM (Im et al. 1998; Brooks et al. 1983). The solution of the Poisson–Boltzmann equation is the electrostatic potential $\phi(\mathbf{r})$ which can be expressed as a potential that is composed of two parts

$$\phi(\mathbf{r}) = \sum_{i=1}^{M} \frac{q_i}{4\pi\varepsilon_p|\mathbf{r} - \mathbf{r}_i'|} + \phi_{\mathrm{rf}}(\mathbf{r}) \quad (2)$$

The first term in Eq. 2 describes the Coulomb electrostatic potential at the position $\mathbf{r}$ caused by M point charges q_i at positions $\mathbf{r}_i'$ in a medium with a dielectric permittivity ε_p, the term $\phi_{\mathrm{rf}}(\mathbf{r})$ describes the reaction field potential originating from the dielectric boundary between the protein and the solvent as well as from the distribution of ions in the solution. The reaction field is caused by the polarization of the environment. Two polarization effects can be distinguished: (i) the electronic polarization, which is caused by the polarization of the electron cloud in the electrostatic field of the solute, and (ii) the orientational polarization, which is caused by the reorientation of solvent molecules in the electrostatic field of the solute. The reaction field is always oriented opposite to the field of the solute, and therefore it shields the field of the solute. This reaction field is of great importance for understanding the structural and functional properties of proteins. For instance, in aqueous solution the dipole of a peptide α-helix is counteracted by the reaction field, which drastically reduces the strength of the helix dipole compared to its value in vacuum (Sengupta et al. 2005a). Moreover, reaction field effects can explain the orientation of helices in membrane proteins (Sengupta et al. 2005b).

The electrostatic potential that is obtained by solving the Poisson–Boltzmann equation has already a great value by itself. Visualization of this potential can give first insights into the interaction between molecules as shown for instance in Fig. 3 where the electrostatic potential of the electron transfer partners plastocyanin and cytochrome *f* is depicted. Furthermore, the electrostatic potential can also be used to calculate electrostatic energies. Such calculations can give quantitative insights into biochemical mechanisms. Two different kind of electrostatic energies can be distinguished. The first kind of energy is the interaction energy G_{inter} between two disjunct sets of charges $\{q\}$ and $\{p\}$, which is calculated by

$$G_{\mathrm{inter}} = \sum_{i=1}^{N_q} q_i\phi(\{p\}, \mathbf{r}_{q_i}) = \sum_{i=1}^{N_p} p_i\phi(\{q\}, \mathbf{r}_{p_i}) \quad (3)$$

where N_q and N_p are the number of charges in the charge sets $\{q\}$ and $\{p\}$, respectively, $\phi(\{p\}, \mathbf{r}_{q_i})$ is the potential caused by the charge set $\{p\}$ at the position of the charge q_i, and $\phi(\{q\}, \mathbf{r}_{p_i})$ is the potential caused by the charge set $\{q\}$ at the position of the charge p_i. As can be seen from Eq. 3, this interaction energy is symmetric. The second kind of energy is the interaction energy of the charge set $\{q\}$ with its own reaction field potential ϕ_{rf} which is given by

$$G_{\mathrm{rf}} = \frac{1}{2}\sum_{i=1}^{N_q} q_i\phi_{\mathrm{rf}}(\{q\}, \mathbf{r}_{q_i}) \quad (4)$$

The factor $\frac{1}{2}$ is due to the linear response ansatz that is used to obtain this energy (Daune 1999).

The model resulting from the continuum electrostatic approach, although simple at a first sight, is extremely successful in describing the electrostatic properties of proteins and it can be applied to various biochemical problems as will be detailed below.

Applications of the continuum electrostatic model

Association of proteins

Biochemical processes depend on the ability of proteins to interact with each other, with nucleic acids, with lipids, with polysaccharides, and with substrate molecules. Specific molecular recognition is a prerequisite for electron

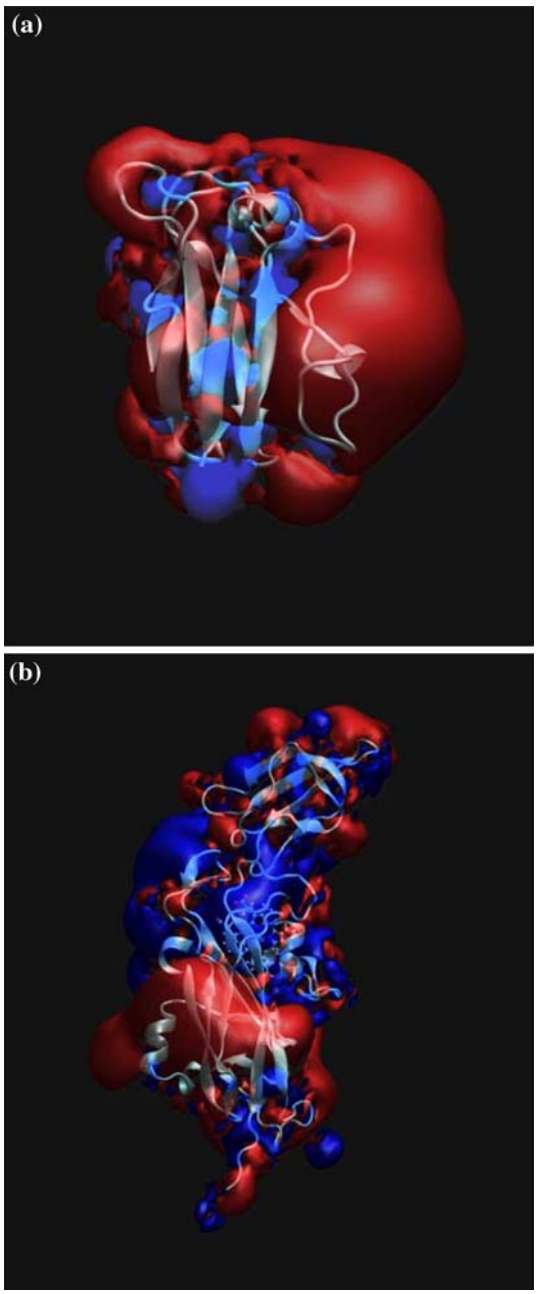

Fig. 3 Visualization of the electrostatic potential of the two electron transfer partners plastocyanin (**a**) and cytochrome *f* (**b**). The electrostatic potential contours at 1 k_BT (blue) and -1 k_BT (red) are shown. The large red region (negative potential) in plastocyanin depicts the acidic patch. This acidic patch is involved in the association with cytochrome *f*. The blue region (positive potential) on the left side of cytochrome *f* depicts the docking region on this protein. The electrostatic complementarity of these proteins is the reason for the association of these two molecules. The potentials were calculated with APBS and visualized with VMD

transfer between redox partners, for signal transduction in cells, for the adaptation of cells to environmental conditions, and for many other physiological reactions. Therefore, the understanding of protein association is required to elucidate biochemical processes. Continuum electrostatic calculations are suitable to investigate the interaction between proteins. In bioenergetic reactions, the interaction of electron transfer proteins is of particular interest. Since electron transfer proteins often associate only transiently, it is difficult to analyze their association experimentally. Therefore, theoretical methods are especially valuable for these systems to obtain structural information about these protein complexes.

Docking of electron transfer proteins

One photosynthetic electron transfer complex that was extensively studied theoretically is the complex formed between plastocyanin and cytochrome *f* (Ullmann et al. 1997b; Pearson et al. 1996; De Rienzo et al. 2001). In the first docking study on this complex, the association of plastocyanin and cytochrome *f* was analyzed in four steps (Ullmann et al. 1997b, Fig. 4). In the first step, Monte Carlo sampling was used to generate docked complexes. In this step, one protein moves in the electrostatic potential of the other protein. Low energy configurations are accepted according to the Metropolis criterion (Metropolis et al. 1953). In the second step, the resulting molecular configurations with relatively low energies were grouped into families by a cluster algorithm. In the third step, the configurations having the lowest energies, one from each family, were used as starting points of a molecular dynamics simulation. Hydration was considered explicitly in these simulations. In the fourth step, the complexes were analyzed in terms of their association energy and in terms of their electron transfer efficiency. The association energy was calculated with a thermodynamic cycle using energies obtained from the Poisson–Boltzmann equation. The electron transfer efficiency between the copper and heme sites was analyzed and compared by the *Pathways* method (Betts et al. 1992; Beratan et al. 1985, 1989, 1990, 1991; Ullmann and Kostić 1995). Interestingly, the complex with the most stable configuration did not display the most efficient path for electron transfer, thus, a rearrangement of the complex is required in order to enable electron transfer. Such a rearrangement is in agreement with experimental results (Qin and Kostić 1993) obtained on this complex. The strategy that was followed to analyze computationally the complex between plastocyanin and cytochrome *f* allowed to get a detailed understanding of the electron transfer mechanism on a structural basis and enabled to explain experimental results. Therefore it can be seen as a paradigm for the analysis of electron transfer protein complexes. An NMR study of the interaction of plastocyanin and cytochrome *f* confirmed the model that was proposed based on the Monte Carlo simulations (Ubbink et al. 1998).

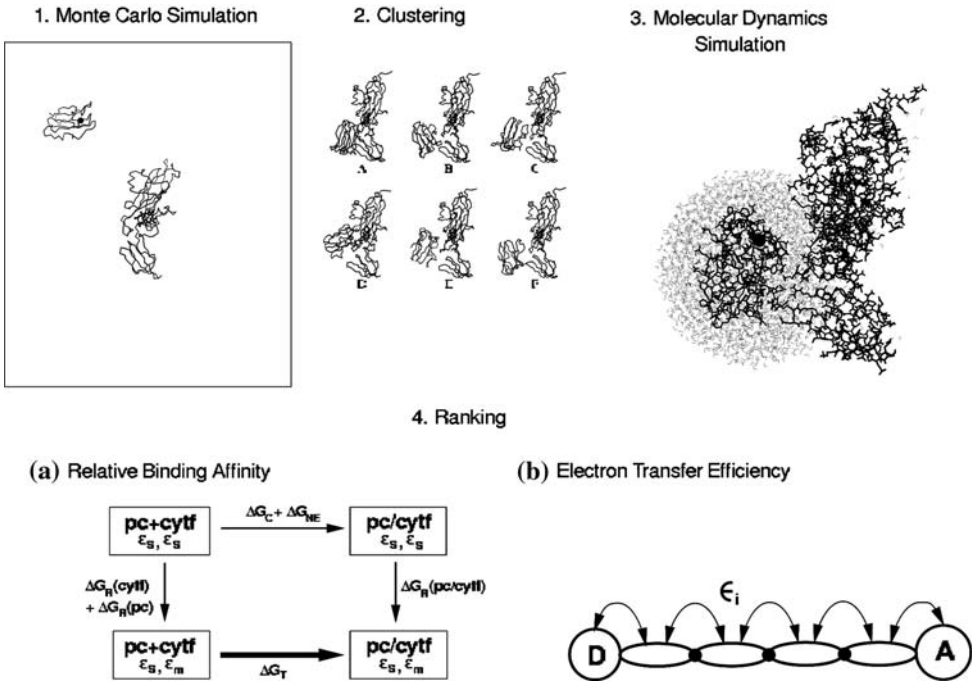

Fig. 4 Simulation of the association of plastocyanin and cytochrome *f*. The association of electron transfer proteins is simulated in several stages. Many encounter trajectories of plastocyanin and cytochrome *f* are generated by a Monte Carlo simulation (1). The molecular configurations having relatively low energies are grouped by structural similarity into several families (2). Configurations having the lowest energies are subjected to a thorough molecular dynamics simulation (3). The hydration of the proteins was treated explicitly. Finally a ranking of the different complexes is performed (4). The energy of binding is calculated using the Poisson–Boltzmann equation (4a). The electron transfer efficiency between the copper and heme sites was analyzed and compared by the *Pathways* method (4b)

A similar strategy was used to study the complex between plastocyanin and cytochrome *c*. Although this complex has no physiological relevance, its features make it a good test system and led to the understanding of the dynamics of electron transfer proteins. This protein complex shows an electron transfer dynamics that is largely influenced by environmental conditions such as solvent viscosity and ionic strength (Kostić 1996; Zhou and Kostić 1993). Using different theoretical approaches including electrostatic calculations, and Monte Carlo simulations, it was possible to elucidate the structural basis of the behavior of this diprotein complex (Ullmann and Kostić 1995; Roberts et al. 1991). The theoretical investigations performed on this complex helped to interpret the experimental data on mutations and pH effects (Ivković-Jensen et al. 1998, 1999; Sokerina et al. 1999; Crnogorac et al. 2001).

Brownian dynamics simulations are in some respect similar to the Monte Carlo approach described above for plastocyanin and cytochrome *f* (Madura et al. 1994; Gabdoulline and Wade 2002; Andrew et al. 1993; Northrup et al. 1984; Northrup 1994). In Brownian dynamics simulations, the association of two proteins is simulated using Newton's equations of motion combined with additional random and friction terms and the interaction is calculated based on electrostatic potentials obtained from the Poisson–Boltzmann equation. Brownian dynamics simulations enable to determine relative association rate constants and thus to study for instance the influence of mutations or of ionic strength on association rates. These simulations have been also applied to a variety of photosynthetic electron transfer complexes and allowed to interpret experimental findings on the association between electron transfer partners (Pearson and Gross 1995; Pearson et al. 1996; De Rienzo et al. 2001; Haddadian and Gross 2006; Gross and Rosemberg 2006; Haddadian and Gross 2005).

Comparison of electron transfer proteins based on their electrostatic potentials

Proteins which perform similar functions have often similar structures. However, exceptions to this rule can be found and two of these exceptions play a prominent role in photosynthetic electron transfer of some cyanobacteria and uni-cellular algae (Ubbink 2004; Hervás et al. 2003). Under copper deficiency, the blue copper protein plastocyanin is replaced by the heme protein cytochrome c_6, and under iron deficiency, the iron-sulfur protein ferredoxin is replaced by the flavoprotein flavodoxin. Although the replacing proteins differ in composition and structure, they

perform the same function in the photosynthetic electron-transport chain as the original proteins.

In order to understand the structural basis of their functional equivalence, the isofunctional proteins can be compared on the basis of their electrostatic potentials (Ullmann et al. 1997a, 2000). The molecules can be superimposed by optimizing the similarity of their electrostatic potentials with respect to their relative orientation. The integral-based Hodgkin index H_{ab}^{elec} (Hodgkin and Richards 1987) is ideal for defining the similarity of two electrostatic potentials.

$$H_{ab}^{\text{elec}} = \frac{2\int \phi_a \phi_b \mathrm{d}\, V}{\int \phi_a^2 \mathrm{d}\, V + \int \phi_b^2 \mathrm{d}\, V} \tag{5}$$

The potentials ϕ of the structurally different molecules a and b are integrated over the whole volume V. The numerator quantifies the spatial overlap of the electrostatic potentials ϕ, while the denominator normalizes this value. The resulting similarity index falls in the interval between -1 and $+1$. The value $+1$ corresponds to molecules with identical potentials, whereas -1 corresponds to electrostatic complementarity, i.e., potentials of the same magnitude but opposite sign. In order to optimize the superposition of the two molecules, the Coulomb potentials are approximated by Gaussian potentials and Eq. 5 is minimized with respect to the relative orientation of the two molecules (Ullmann et al. 2000). This structural superposition can be used to identify functionally equivalent residues.

On the basis of the superposition of electrostatic potentials, it was possible to elucidate the reasons of the functional equivalence of plastocyanin and cytochrome c_6 and of ferredoxin and flavodoxin (Fig. 5). In particular, the association and the electron-transfer reactions with their physiological reaction partners could be analyzed. Interestingly, functional analogous amino acids enabling specific recognition and efficient electron transfer could be identified for both couples of isofunctional proteins (Ullmann et al. 1997a, 2000).

Tuning of absorption spectra

Chromophore-binding proteins can tune the absorption of their chromophore to an exact maximum by specific interactions. This is for instance the case for rhodopsins which bind a retinal as a chromophore. The absorption maxima in this protein family range from ultraviolet to far red. The shift of the absorption maxima between the different rhodopsins is called inter-protein shift. Archaeal rhodopsins represent good test systems for theoretical studies on chromophore tuning since high-resolution structures of these proteins are available. Moreover, many experimental data from mutational studies exist.

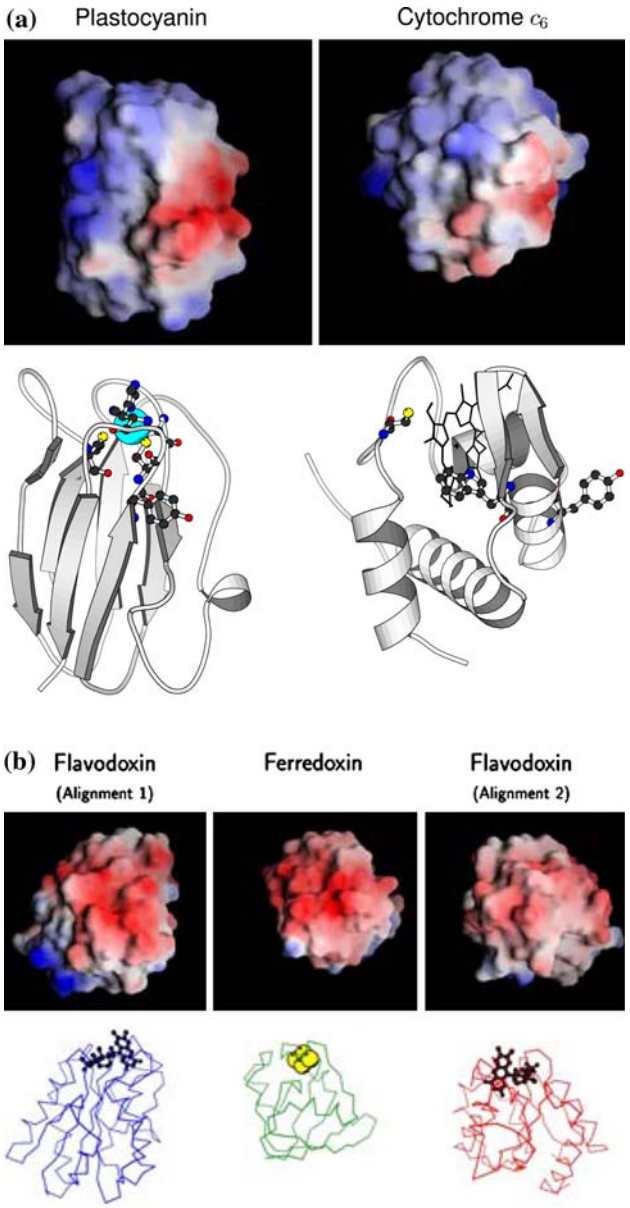

Fig. 5 (**a**) Electrostatic potential of plastocyanin (left) and cytochrome c_6 (right) from *C. reinhardtii* mapped to the protein surface. The lower panel shows a ribbon presentation of the two proteins. The orientation of the two molecules corresponds to their superposition in which their electrostatic potentials match best. It can be seen that the proteins do not share any similarity in the secondary structural level. However, surface residues that are involved in electron transfer and association are functionally conserved. These residues are Tyr83 and the copper ligand His87 in plastocyanin, and Trp63 and Cys17 bound to the heme in cytochrome c_6. (**b**) Electrostatic potential of ferredoxin and flavodoxin from *Anabaena PCC 7210*. The orientation of flavodoxin (Alignment 1 and Alignment 2) shows the best matches of the potentials of flavodoxin with the potential of ferredoxin. These two orientations are related by a 180° rotation. The lower panel shows a wire frame model of the Cα chain of the proteins. The proteins show no significant similarities in their structures and they even differ in size. Nevertheless, the surface region relevant for association and electron transfer show similar features. The potentials are calculated with APBS and visualized with VMD

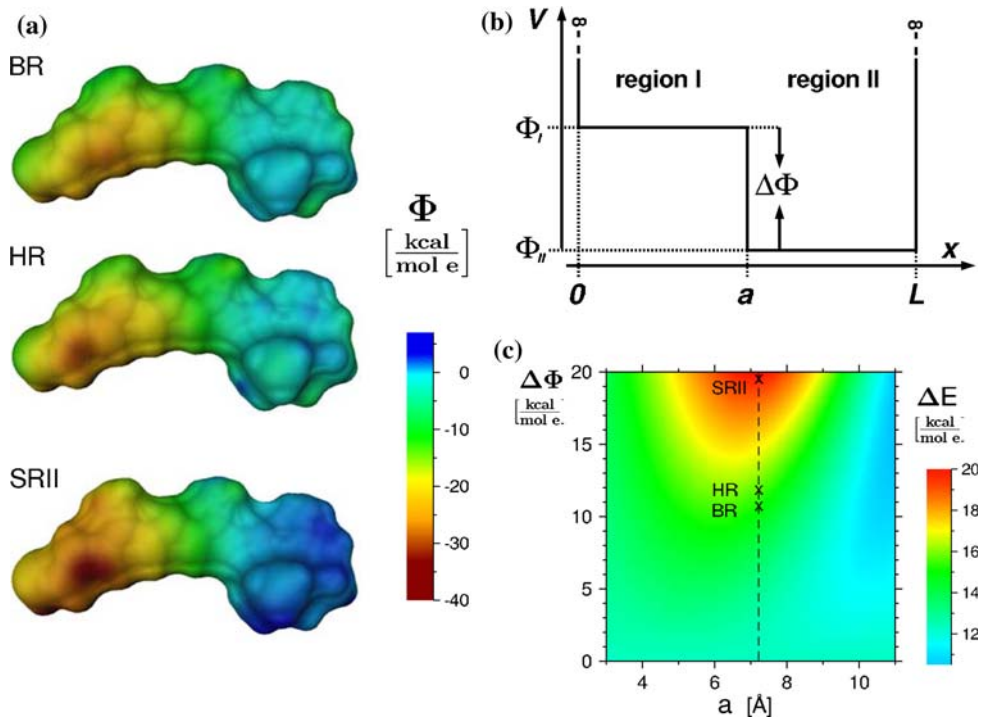

Fig. 6 (**a**) Electrostatic potential of BR, HR, and SRII. The potential is plotted at the van der Waals surface of the retinal Schiff base. The magnitude of the potential is color coded. It can be seen that the electrostatic potential of BR and HR are more similar to each other compared to the potential of SRII. In SRII, the potential along the retinal varies more strongly. This stronger variation can explain the difference in the absorption maxima of the proteins. The potentials were calculated with APBS and visualized with VMD. (**b**) Quantum mechanical model of a particle in a box with a step potential. L is the length of the box, a the position of the step, Φ_I and Φ_{II} is the potential in region I and region II, respectively, and $\Delta\Phi$ denotes the height of the potential step. (**c**) Dependence of the first ($S_0 \rightarrow S_1$) excitation energy ΔE on the position of the step a and the potential difference $\Delta\Phi$ using the quantum mechanical model of a particle in a box with potential step. The excitation energy ΔE, given in kcal mol^{-1} e^{-1}, is color coded. The dashed line marks the position of the step in the archaeal rhodopsins. The crosses indicate the height of the potential step $\Delta\Phi$ for BR, HR, and SRII. It can be seen that the position and the height of the potential step can efficiently tune the absorption maximum

The inter-protein shift between archaeal rhodopsins may in principle originate from differences in either steric or electrostatic interaction between the protein and the chromophore. However, experimental data (Harbison et al. 1985; Baselt et al. 1989; Sakamoto et al. 1998; Belrhali et al. 1999; Luecke et al. 1999, 2001; Royant et al. 2001; Kandori et al. 2001) and theoretical studies (Ren et al. 2001; Hayashi et al. 2001) demonstrate that differences in chromophore geometry are negligible for the inter-protein shift. Thus, electrostatic interactions between the retinal chromophore and the protein appear to be a major determinant for spectral shifts between different rhodopsins (Ren et al. 2001; Hayashi et al. 2001; Kandori et al. 2001).

Based on the Poisson–Boltzmann equation, the electrostatic potential at the retinal π-system of three archaeal rhodopsins, namely of the proton pump bacteriorhodopsin (BR), the chloride pump halorhodopsin (HR), and signaling protein sensory rhodopsin II (SRII) were computed and compared (Kloppmann et al. 2005). Despite the structural similarity between these three proteins, the absorption maximum of SRII is considerably blue-shifted (maximum at 500 nm) compared to the spectrum of BR and HR (maxima at 570 and 585 nm, respectively). In agreement with their absorption maxima, it can be seen that the electrostatic potential at the retinal is similar for BR and HR, whereas the one of SRII differs significantly (Fig. 6). A variant of the quantum mechanical model of a particle in a box is able to qualitatively relate the differences in the electrostatic potential between the archaeal rhodopsins to differences in their absorption behavior (Kloppmann et al. 2005). The qualitative picture offered by this model reveals an interesting aspect of spectral tuning. As can be seen in Fig. 6, spectral tuning is most effective if the controlling potential changes close to the center of the retinal π-system: then, even small changes in the height of the potential step $\Delta\Phi$ have a pronounced influence on the excitation energy ΔE (Fig. 6a). Indeed, the electrostatic potentials of the three archaeal rhodopsins display two potential plateaus (one in the β-ionone ring region and another one in the Schiff base region), and the separation between these two plateaus is located approximately in the middle of the retinal π-system. The difference between these two plateaus can be seen as a

step potential. For SRII, the excitation energy is significantly higher than for BR and HR, which instead have similar excitation energies. The model of a particle in a box with a step potential reproduces the general trend of the measured absorption maxima by grouping BR and HR together and showing a significantly higher excitation energy for SRII. This finding indicates that the observed differences in electrostatic potential in BR, HR, and SRII are related to differences in the absorption maxima. To understand the structural basis of the differences between BR, HR, and SRII, the electrostatic potential can be decomposed into individual components. Seven residues that can account for the difference among the electrostatic potential of the proteins could be identified. The analysis of the electrostatic potential at the retinal can thus not only point out the differences among the different archaeal rhodopsins, but it can also help to identify individual residues that cause these differences.

Tuning of absorption spectra is not only important in rhodopsins, but also in photosynthetic reaction centers and in light harvesting complexes in photosynthesis. On one hand, tuning of the absorption spectra is important for adaptation to different ecological niches (Cogdell et al. 2006). On the other hand, the pigments in light harvesting complexes need to have the appropriate spectra to allow efficient energy channeling into the photochemically active pigment. Also in these proteins, electrostatic interaction plays a prominent role in the tuning of absorption spectra (Adolphs and Renger 2006; Madjet et al. 2006; Sener et al. 2004). Electrostatic calculations in combination with quantum chemical calculations (Adolphs and Renger 2006; Liu et al. 2004; Ritz et al. 2002; Hu et al. 2002; Cogdell et al. 2006) can help to give deeper insights into this intricate problem.

Coupling of protonation and reduction in proteins

The coupling of protonation and reduction is a common feature in many bioenergetic reactions. Often exergonic electron transfer reactions are coupled to endergonic proton transfer reactions to build up electrochemical gradients across a membrane which are then used by ATP-synthase to produce ATP. The understanding of the coupling between electrons and protons on a structural level is thus a central problem in bioenergetic research. For the theoretical description, two cases have to be distinguished: (i) The protonation or redox energies of model compounds of the groups are known from experiments and the shifts due to the protein environment needs to be calculated. This scenario is for instance fulfilled in many heme proteins such as for instance cytochrome c_3 and in part also for the Q_B reduction in bacterial photosynthetic reaction centers. (ii) The protonation or redox energies of model compounds are not known experimentally but can be calculated quantum chemically. This scenario is for instance fulfilled for the Rieske iron-sulfur center. The first scenario can be modeled by microstate description including only electrostatic interactions, the second scenario can be modeled by a combined electrostatic and quantum chemical approach.

Microstate model

We consider a system that possesses N protonatable sites and K redox-active sites. Such a system can adopt $M = 2^{N+K}$ states assuming that each sites can exist in two forms. The interaction between them can be modeled purely electrostatically, i.e., the electronic coupling is negligible. Each state of the system can be written as an $N + K$-dimensional vector $\vec{x} = (x_1, \ldots, x_{N+K})$, where x_i is 0 or 1 if site i is deprotonated (reduced) or protonated (oxidized), respectively. Each state of the system has a well-defined energy which depends on the energetics of the individual sites and the interaction between sites. The energy of a state $\vec{x}_\nu$ is given by (Bashford and Karplus 1990; Ullmann and Knapp 1999; Ullmann 2000; Gunner et al. 2006; Nielsen and McCammon 2003):

$$\begin{aligned} G(\vec{x}_\nu) = &\sum_{i=1}^{N}(x_{\nu,i} - x_i^\circ)RT\ln 10(\mathrm{pH} - \mathrm{p}K_{a,i}^{\mathrm{intr}}) \\ &- \sum_{i=1}^{K}(x_{\nu,i} - x_i^\circ)F(E - E_i^{\mathrm{intr}}) \\ &+ \frac{1}{2}\sum_{i=1}^{N+K}\sum_{j=1}^{N+K}(x_{\nu,i} - x_i^\circ)(x_{\nu,j} - x_j^\circ)W_{ij} \end{aligned} \tag{6}$$

where R is the gas constant; T is the absolute temperature; F is the Faraday constant; $x_{\nu,i}$ denotes the protonation or redox form of the site i in state $\vec{x}_\nu$, x_i° is the reference form of site i; $\mathrm{p}K_{a,i}^{\mathrm{intr}}$ and E_i^{intr} are the $\mathrm{p}K_a$ value and redox potential, respectively, that site i would have if all other sites are in their reference form (intrinsic $\mathrm{p}K_a$ value and intrinsic redox potential); E is the reduction potential of the solution; pH is the pH value of the solution; W_{ij} represents the interaction of site i with site j. The energetic parameters $\mathrm{p}K_{a,i}^{\mathrm{intr}}$ and E_i^{intr} are calculated using electrostatic methods from the $\mathrm{p}K_a$ value or redox potential of a model of the respective groups in aqueous solution and the shift of these values due to the protein environment. The interaction energy W_{ij} between the groups can be calculated by an electrostatic approach (Bashford and Karplus 1990; Ullmann and Knapp 1999; Borodich and Ullmann 2004).

Equilibrium properties of a physical system are completely determined by the energies of its states. To keep the notation concise, states will be numbered by Greek indices; i.e., for state energies we write G_ν instead of $G(\vec{x}_\nu)$. For site indices, the roman letters i and j will be used. The equilibrium probability of a single state $\vec{x}_\nu$ is given by

$$P_v^{\mathrm{eq}} = \frac{\mathrm{e}^{-\beta G_v}}{Z} \tag{7}$$

with $\beta = 1/RT$ and Z being the partition function of the system.

$$Z = \sum_{v=1}^{M} \mathrm{e}^{-\beta G_v} \tag{8}$$

The sum runs over all M possible states. Properties of single sites can be obtained from Eq. 7 by summing up the individual contributions of all states. For example, the probability of site i being protonated is given by

$$\langle x_i \rangle = \sum_{v}^{M} x_{v,i} P_v^{\mathrm{eq}} \tag{9}$$

where $x_{v,i}$ denotes the protonation form of site i in the charge state $\vec{x}_v$. For small systems, this sum can be evaluated explicitly. For larger systems, Monte–Carlo techniques can be used to determine these probabilities (Beroza et al. 1991).

For a system of interacting sites, the probabilities $\langle x_i \rangle$ can show a complex shape, thus rendering the assignment of mid-point potentials difficult or even meaningless (Ullmann 2003; Onufriev et al. 2001; Onufriev and Ullmann 2004; Klingen and Ullmann 2006). The energy differences between microstates, however, remain well defined and thus form a convenient basis to describe the system.

Proton uptake upon Q_B reduction in the bacterial photosynthetic reaction center

The reduction of Q_B in the photosynthetic reaction center leads to a change of the protonation probabilities of residues in its vicinity. This change has been extensively investigated by the theoretical approach described above (Koepke et al. 2007; Rabenstein and Ullmann 1998; Rabenstein et al. 1998; Alexov and Gummer 1999; Ishiktia and Knapp 2005; Alexov et al. 2000; Rabenstein et al. 2000; Taly et al. 2003; Beroza et al. 1991). As a central protein of photosynthesis, the reaction center converts light energy into chemical energy. Two electrons are transferred one after the other from the special pair, a bacteriochlorophyll dimer, via a series of electron donor and acceptor groups to a coenzyme Q molecule called Q_A and from there to the terminal electron acceptor, another coenzyme Q molecule called Q_B. Upon reduction, two protons are taken up from the bulk and are transferred to Q_B via one or several proton transfer pathways (Sebban et al. 1995; Abresch et al. 1998; Baciou and Michel 1995; Takahashi and Wraight 1992; Ädelroth et al. 2001; Paddock et al. 2001).

In the 1980s, it was commonly believed that first the two electrons are transferred to Q_B and then Q_B gets protonated. This mechanism would involve the occurrence of the doubly reduced unprotonated quinol Q_B^{2-} during the reaction. Later, kinetic, spectroscopic, and mutational studies suggested that the first electron transfer is coupled with a proton transfer to $Q_B^{\cdot -}$ (Graige et al. 1996; Paddock et al. 1990; Hienerwadel et al. 1995). In line with these experimental results, electrostatic calculations showed that the reaction energy for the second electron transfer ($Q_A^{\cdot -} Q_B^{\cdot -} \longrightarrow Q_A Q_B^{2-}$) is extremely endergonic (Rabenstein and Ullmann 1998; Rabenstein et al. 1998) indicating that the Q_B^{2-} is a thermally inaccessible intermediate. Consequently, the second electron transfer will not occur before the protonation of $Q_B^{\cdot -}$.

Two alternative positions of Q_B, distal and proximal to the non-heme iron, were resolved crystallographically (Stowell et al. 1997). Electrostatic calculations on the reaction center of *Rhodobacter sphaeroides* showed that the first electron transfer ($Q_A^{\cdot -} Q_B \longrightarrow Q_A Q_B^{\cdot -}$) is uphill when Q_B is in the distal position and downhill when Q_B is in the proximal position (Rabenstein et al. 2000; Alexov and Gummer 1999). Thus, the electron transfer to Q_B is influenced by a rearrangement from an electron transfer inactive state to an electron transfer active state.

Theoretical investigations based on the model including only pure electrostatic interaction allowed to identify a cluster of strongly coupled residues, namely AspL210, AspL213, and GluL212 (Fig. 7), which are changing their protonation after the first reduction of Q_B (Alexov et al. 2000; Rabenstein et al. 2000; Alexov and Gunner 1999; Taly et al. 2003). In addition, the involvement of SerL223, a hydrogen-bond partner of Q_B (Fig. 7), in the proton transfer (Alexov and Gunner 1999) and in the tuning of the redox potential of Q_B (Ishikita and Knapp 2004) were also proposed from electrostatic calculations. The importance of SerL223, AspL213, GluL212, and AspL210 for the proton transfer was also found by experimental studies (Paddock et al. 1989, 1997, 2003; Ädelroth et al. 2001; Okamura et al. 2000). The mutation of these residues can lead to photoinactive reaction center proteins (for example AspL213 → Asn). However in some cases, the function of the reaction center can be restored by second site mutations (for example ArgM233 → Cys) (Paddock et al. 1994; Paddock et al. 1998; Miksovska et al. 1997). For the double mutant (AspL213 → Asn, ArgM233 → Cys), Ishiktia and Knapp (2005) calculated shifts of proton binding constants of several other residues leading to an alternative proton transfer pathway from the aqueous solution to the Q_B binding site. Thus, these calculations offered a molecular mechanism to understand the proton transfer in this so-called revertant mutant. Theoretical calculations on the protonation events coupled to Q_B reduction have largely influenced the thinking about the proton transfer reactions in this protein. These theoretical studies have led to many testable hypotheses which in part have been already proven experimentally.

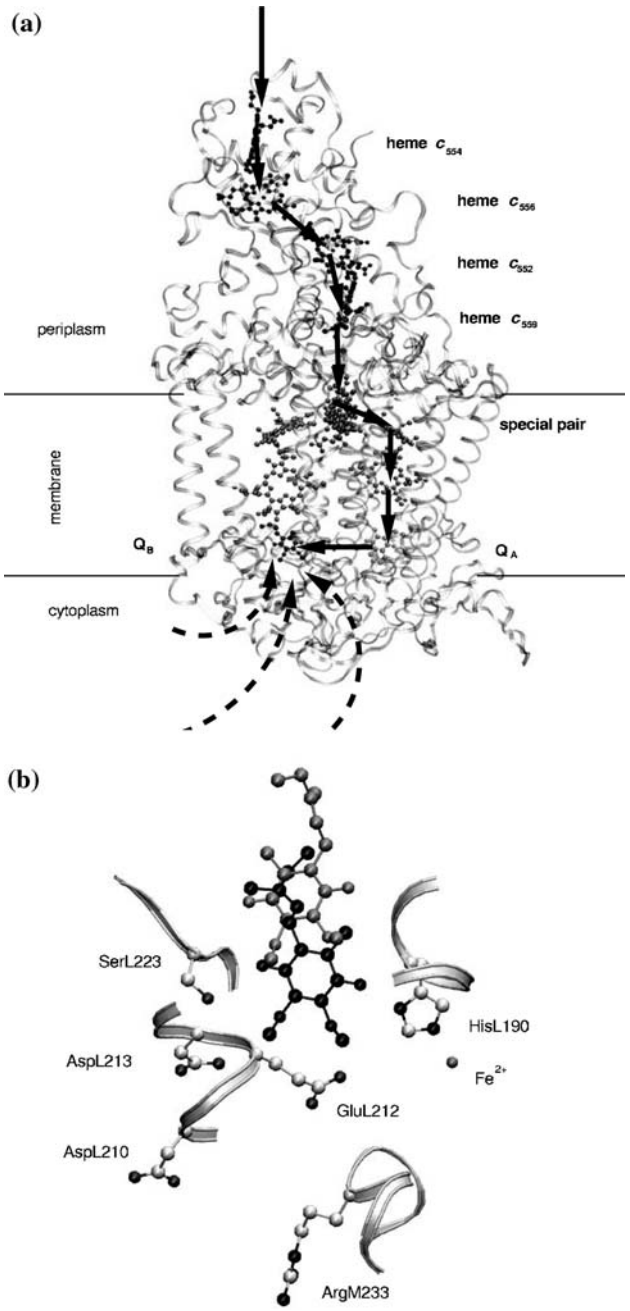

Fig. 7 The photosynthetic reaction center. (**a**) Electron (solid arrows) and proton transfer (dashed arrows) in the photosynthetic reaction center of *Blastochloris viridis*. The special pair, the other electron transfer groups, and the two quinone sites (Q_A and Q_B) are shown. (**b**) The binding positions for ubiquinone in the Q_B binding site of the reaction center of *Rhodobacter sphaeroides*; ubiquinone can be either bound distally (light gray) or proximally (dark gray) to the iron. Additionally important residues for the proton transfer are depicted. The letters M and L in the residue name indicate the subunit to which the residue belongs

Quantum chemical calculation of absolute pK_a values and redox potentials

The microstate model described above considers purely electrostatic interaction between the sites. Such a model is applicable to many proteins. However, it fails in some cases, for instance when protons bind directly to a redox-active site. Under the condition of strong electronic coupling between the proton binding site and the redox-active center, often experimental data for pK_a values or redox potentials of appropriate model compounds do not exist. Thus, the microscopic equilibrium constants need to be calculated by a quantum mechanical approach (Li et al. 1998, 1996; Ullmann et al. 2002). The pK_a values relate directly to the free energy of deprotonation in aqueous solution $\Delta G^{\text{deprot}}_{\text{water}}$ by Eq. 10. $\Delta G^{\text{deprot}}_{\text{water}}$ can be expressed as a sum of two contributions: the solvation energy difference $\Delta\Delta G^{\text{deprot}}_{\text{solv}}$ between the associated and the dissociated systems and the gas phase deprotonation energy $\Delta G^{\text{deprot}}_{\text{vac}}$.

$$\begin{aligned} pK_a &= \frac{1}{\ln 10\, k_B T}\Delta G^{\text{deprot}}_{\text{water}} \\ &= \frac{1}{\ln 10\, k_B T}\left(\Delta G^{\text{deprot}}_{\text{vac}} + \Delta\Delta G^{\text{deprot}}_{\text{solv}}\right) \end{aligned} \tag{10}$$

The solvation energy difference $\Delta\Delta G^{\text{deprot}}_{\text{solv}}$ is obtained from Eq. 11.

$$\Delta\Delta G^{\text{deprot}}_{\text{solv}} = \Delta G_{\text{solv}}(\text{A}^-) + \Delta G_{\text{solv}}(\text{H}^+) - \Delta G_{\text{solv}}(\text{AH}) \tag{11}$$

The solvation energy of the protonated and deprotonated molecule, $\Delta G_{\text{solv}}(\text{AH})$ and $\Delta G_{\text{solv}}(\text{A}^-)$, can be calculated from the solution of the Poisson–Boltzmann equation. The solvation energy of a proton $\Delta G_{\text{solv}}(\text{H}^+)$ can be obtained from the experimentally measured potential of the standard hydrogen electrode (Reiss and Heller 1985). The gas phase protonation energy $\Delta G^{\text{deprot}}_{\text{vac}}$ can be calculated from Eq. 12,

$$\begin{aligned} \Delta G^{\text{deprot}}_{\text{vac}} = {} & \Delta H^{\text{deprot}}_{\text{vac}} + \Delta H^{\text{deprot}}_{\text{vib}} + H_{\text{trans}}(\text{H}^+) \\ & + \Delta(pV) - T[S(\text{H}^+)] \end{aligned} \tag{12}$$

where $\Delta H^{\text{deprot}}_{\text{vac}}$ is the difference in the vacuum energy of the associated (protonated) and dissociated (deprotonated and hydrogen ion) system as calculated by quantum chemical methods; $\Delta H^{\text{deprot}}_{\text{vib}}$ is the change in the vibrational energy between the protonated and deprotonated state; $H_{\text{trans}}(\text{H}^+)$ is the translational energy of a proton which is $\frac{3}{2}RT$; $\Delta(pV)$ is the energy change due to the volume change in the gas phase reaction which is estimated to be RT from the ideal gas approximation; and $T[S(\text{H}^+)]$ is the entropic portion of the gas-phase free energy of a proton which can be derived from the Sackur-Tetrode equation (Hill 1960).

The redox potential $E^{\text{o}}_{\text{redox}}$ can be computed by a similar approach using Eq. 13

$$E^{\text{o}}_{\text{redox}} = \frac{1}{F}\left(\Delta H^{\text{redox}}_{\text{vac}} + \Delta\Delta G^{\text{redox}}_{\text{solv}}\right) + \Delta\text{SHE} \tag{13}$$

where $\Delta H^{\text{redox}}_{\text{vac}}$ is the difference in the vacuum energy between the oxidized and the reduced states; $\Delta\Delta G^{\text{redox}}_{\text{solv}}$ is the difference in interaction energy with the protein and the

solvent between the oxidized and the reduced states and is calculated analogously to Eq. 11; F is the Faraday constant; and ΔSHE is the standard potential of the hydrogen electrode.

Coupling of protonation and reduction in the Rieske protein

Rieske proteins are metalloproteins for which reduction and protonation are strongly coupled. These proteins are iron-sulfur proteins that contain a [2Fe2S] cluster coordinated by two cysteine and two histidine residues (Fig. 8). The iron-sulfur center can undergo one-electron redox-reactions, with the two iron atoms being formally Fe(III) in the oxidized state of the cluster. The redox potential of this transition has been shown to be pH-dependent, and the pH-dependence has been tentatively associated with a redox-dependence of the protonation of the ligand histidines that reversibly protonate at their N_ε atoms (Link 1994; Zu et al. 2001). Such a coupling between the redox-state of the center and the protonation of the ligand histidines could be clearly established from a quantum-chemical characterization of the cluster (Ullmann et al. 2002; Leggate et al. 2004). Since the redox-active orbitals are delocalized over the whole iron-sulfur center including the histidine ligands, a model based on pure electrostatic interactions is not suitable. Instead, electronic coupling needs to be considered. Density functional calculations showed that the reduced state of the center favors the protonated state of the two histidine ligands, and vice versa. The two redox-dependent macroscopic pK-values of the Rieske protein in bovine cytochrome bc_1 could be calculated from Poisson–Boltzmann electrostatics (Ullmann et al. 2002) and agree well with experimental data (Link 1994; Denke et al. 1998; Lin et al. 2006).

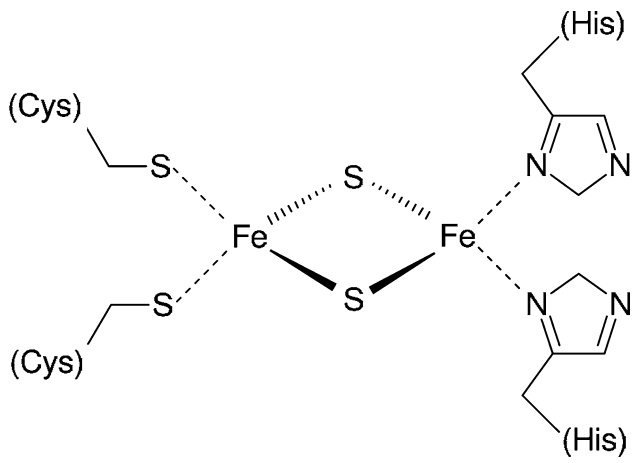

Fig. 8 The chemical structure of the Rieske iron-sulfur cluster. The [2Fe2S] core and coordinating histidine and cysteine sidechains are shown

Rieske proteins are commonly classified into low potential and high potential Rieske proteins. High potential Rieske proteins are found in the cytochrome *bc* complexes that are quinol-oxidizing proton-translocating transmembrane complexes of the photosynthetic and respiratory electron transfer chains. Low potential Rieske proteins occur in bacterial oxygenases that are involved in the degradation of aromatic compounds. High potential Rieske proteins differ from low potential Rieske proteins not only in their redox potentials, but they have also different macroscopic pK-values. In their oxidized state, high potential Rieske proteins titrate in the physiological pH-range, while low potential Rieske proteins have higher pK-values and are protonated at physiological pH. This difference in pK-values could be assigned to differences in the hydrogen bonding pattern and in the distribution of negatively charged residues in a low and a high potential Rieske protein studied by Poisson–Boltzmann electrostatics (Klingen and Ullmann 2004). Two hydrogen bonds toward the Rieske cluster in bovine cytochrome bc_1 stabilize the negative charge in the cluster and therefore contribute to the lower pK-values of the cluster in this high potential Rieske protein. In the low potential Rieske protein of a bacterial biphenyl-dioxygenase (Colbert et al. 2000), several negatively charged residues in the vicinity of the cluster destabilize the negative charge in the cluster and therefore raise the protonation probability of the histidine ligands. Since the studied structural differences between the two proteins will affect the redox equilibria of the cluster in the same way as its protonation equilibria, they most likely also account for the observed redox-potential differences.

The redox-dependent change in the protonation probabilities of the histidine ligands in Rieske proteins of *bc* complexes is central to their function in quinol oxidation. A recent study of the cytochrome bc_1 complex from *Saccharomyces cerevisiae* (Klingen et al. 2007) shows that redox-dependent protonation change of the Rieske histidine ligands can occur also in the context of the quinol-oxidizing active site. This result provides further evidence that quinol oxidation in cytochrome *bc* complexes involves coupled electron and proton transfer from the substrate to the Rieske cluster. A similar behavior is expected for the Rieske protein of the cytochrome b_6f complex which is the equivalent of cytochrome bc_1 in photosynthetic electron transfer chain of higher plants.

Influence of membrane potential and pH gradients on membrane protein protonation

Many membrane proteins, especially those involved in bioenergetic reactions, are exposed to different solvent

conditions on the two different sides of the membrane, which lead, for example, to the membrane potential and the pH gradient across the membrane. The membrane potential and the pH gradient are therefore crucial parameters for investigating the titration behavior of a site in a protein embedded in a membrane.

The influence of a membrane potential on the energetics of a membrane protein can be incorporated in the Poisson–Boltzmann theory (Roux 1997). The linearized Poisson–Boltzmann equation (Eq. 1) can be extended to a membrane system with a membrane potential Ψ :

$$\nabla[\varepsilon(\mathbf{r})\nabla\phi(\mathbf{r})] = -\rho_f(\mathbf{r}) + \varepsilon(\mathbf{r})\overline{\kappa}(\mathbf{r})^2[\phi(\mathbf{r}) - \Psi\Theta(\mathbf{r})] \quad (14)$$

where $\phi(\mathbf{r})$ is the electrostatic potential of the system; $\Theta(\mathbf{r})$ is a Heaviside step function which is equal to zero on the extracellular side and equal to one on the cytoplasmic side; $\varepsilon(\mathbf{r})$ defines the dielectric permittivity; $\rho_f(\mathbf{r})$ is the charge density inside the protein; and $\overline{\kappa}^2(\mathbf{r})$ is the modified Debye-Hückel parameter. Assuming a discrete charge distribution, the solution of Eq. 14, i.e., the electrostatic potential $\phi(\mathbf{r})$, can be expressed as

$$\phi(\mathbf{r}) = \sum_{i=1}^{M} \frac{q_i}{4\pi\varepsilon_p|\mathbf{r} - \mathbf{r}_i'|} + \phi_{\mathrm{rf}}(\mathbf{r}) + \Psi\chi_{\mathrm{mp}}(\mathbf{r}) \quad (15)$$

where the first term describes the Coulomb electrostatic potential at the position $\mathbf{r}$ caused by M point charges q_i at positions $\mathbf{r}_i'$ in a medium with a dielectric permittivity ε_p, the term $\phi_{\mathrm{rf}}(\mathbf{r})$ describes the reaction field potential originating from the dielectric boundary between the protein and the solvent as well as from the distribution of ions in the solution, and the term $\Psi\chi_{\mathrm{mp}}(\mathbf{r})$ describes the contribution due to the membrane potential. Here, $\chi_{\mathrm{mp}}(\mathbf{r})$ is a dimensionless function with the property $0 \le \chi_{\mathrm{mp}}(\mathbf{r}) \le 1$, which depends on the dielectric properties of the system and on the ion distribution in the medium but not on the charge distribution within the protein. The function $\chi_{\mathrm{mp}}(\mathbf{r})$ describes how the membrane potential is modulated inside the membrane protein and it may deviate from a simple linear function (Roux 1997).

The equilibrium protonation probability of a membrane protein exposed to a membrane potential and to different pH values at the two sides of the membrane can be calculated as follows. We consider a transmembrane protein that is in equilibrium with two different reservoirs of protons, i.e., the extracellular side, EC, and the cytoplasmic side, CP. The two reservoirs of protons are not in contact with each other, i.e., protons cannot permeate through the membrane or through the protein. The protein has N sites connected to the extracellular side and K sites connected to the cytoplasmic side. None of the sites is connected to both reservoirs, because otherwise the reservoirs would be in contact with each other. This feature is expected in protein performing vectorial pumping. All sites interact electrostatically. Such a system can adopt 2^{N+K} different protonation states.

The energy of the state of such a system can be written as (for details see Bombarda et al. 2006)

$$\begin{aligned} G(\vec{x_v}) = &\sum_{i=1}^{N}(x_{v,i} - x_i^\circ)RT\ln 10\,(\mathrm{pH_{EC}} - \mathrm{p}K_{a,i}^{\mathrm{intr}}) + F\Psi\Gamma_i \\ &+ \sum_{i=1}^{K}(x_{v,i} - x_i^\circ)RT\ln 10\,(\mathrm{pH_{CP}} - \mathrm{p}K_{a,i}^{\mathrm{intr}}) \\ &+ F\Psi(\Gamma_i - 1) \\ &+ \frac{1}{2}\sum_{i=1}^{N+K}\sum_{j=1}^{N+K}(x_{v,i} - x_i^\circ)(x_{v,j} - x_j^\circ)W_{ij} \end{aligned} \quad (16)$$

where $\mathrm{p}K_{a,i}^{\mathrm{intr}}$ is the intrinsic $\mathrm{p}K_a$ value without the influence of a membrane potential, Γ_i describes the relative contribution of the membrane potential to the protonation energy of the site i, $\mathrm{pH_{EC}}$ and $\mathrm{pH_{CP}}$ are the pH values at the extracellular and at the cytoplasmic side of the membrane. This approach can be straightforwardly extended to include redox-active sites as well.

It should be noted that due to the membrane potential, there is an important difference between the sites connected to the cytoplasm and the sites connected to the extracellular region. In Eq. 16, the energetic cost for protonating a given site amounts to $F\Psi\Gamma_i$ for sites connected to the extracellular side, while the cost is $F\Psi(\Gamma_i - 1)$ for sites connected to the cytoplasm. Thus, for a negative membrane potential (Fig. 9a), protonation is favored on the extracellular side ($F\Psi\Gamma_i < 0$), since proton uptake is downhill with regard to the membrane potential. In contrast, protonation of sites connected to the cytoplasm is hindered ($F\Psi(\Gamma_i - 1) > 0$), since proton uptake is uphill with regard to the membrane potential. The influence of the membrane potential on the protonation probability depends clearly on the proton accessibility of a site, i.e., from which side of the membrane the titratable site receives its proton. For example, the more the membrane potential becomes negative, the higher is the protonation probability of a site that receives the proton from the extracellular side of the membrane and the lower is the protonation probability of a site that is connected with the cytoplasm. In fact, a positive charge follows the direction of the decreasing potential.

Regulation of proton pumping in bacteriorhodopsin

A membrane protein for which the effect of membrane potentials was studied is bacteriorhodopsin. This membrane protein of halophilic archaea pumps protons across the membrane using the energy of light and creates a transmembrane proton gradient upon this process. Bacteriorhodopsin was extensively studied by electrostatic

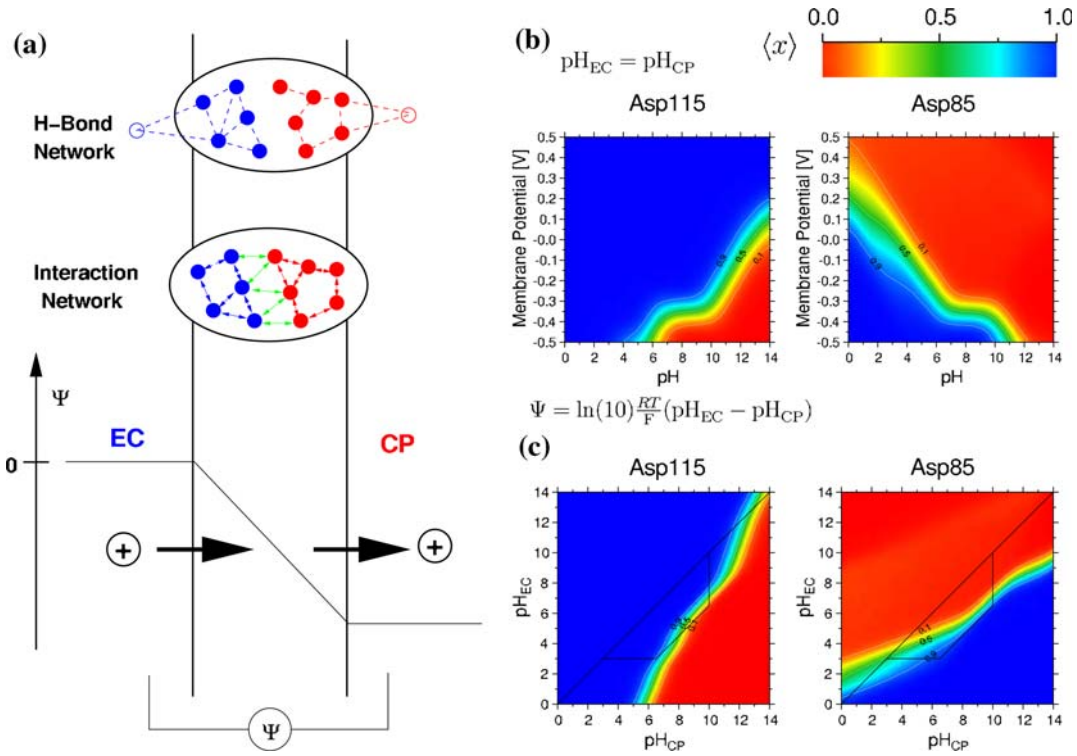

Fig. 9 (**a**) Schematic representation of a membrane protein. In this scheme the membrane potential $\Psi = \psi_{CP} - \psi_{EC} < 0$, with ψ_{CP} and ψ_{EC} being the potential in the cytoplasm (CP) and in the extracellular space (EC), respectively. The membrane protein is depicted as an ellipse. The open circles symbolize the connections of titratable sites to the bulk solvent. The hydrogen bond network relating the titratable sites to the EC region (blue) is not connected to the hydrogen bond network relating the titratable sites to the CP region (red), i.e., protons cannot flow through protein. Proton displacement along one hydrogen bond network is favored in the direction of decreasing potential (black arrows). Under these conditions, the membrane potential will enhance the protonation probability of a titratable site receiving a proton from the EC region (blue) and it will disfavor the protonation of a titratable site receiving a proton from the CP region (red). Due to the electrostatic interaction between sites connected to the extracellular space and sites connected to the cytoplasm (symbolized by the green arrows in the interaction network), the protonation of the sites that are connected to different sides of the membrane are not independent of each other. (**b**, **c**) show the protonation probability of Asp85 and Asp115 in function of membrane potential, pH_{EC} and pH_{CP}. The protonation probability is color-coded as indicated by the color scale on the top of the figure. In (**b**) the effect of the membrane potential is depicted assuming that the pH on the two sides of the membrane is the same. In (**c**) the pH gradient gives rise to a membrane potential. The black line encloses the pH region that was found to be the proton pumping active-region of bacteriorhodopsin

calculations (Bashford and Gerwert 1992; Sampogna and Honig 1994, 1996; Spassov et al. 2001; Onufriev et al. 2003; Song et al. 2003; Scharnagl et al. 1994; Calimet and Ullmann 2004; Bombarda et al. 2006). The analysis of the influence of the membrane potential on the titration behavior of bacteriorhodopsin according to the theory outlined above allowed to shed light on the regulation of its proton pumping. The proton pumping is inhibited when the transmembrane proton gradient becomes larger than 4 pH units. From electrostatic calculations, it can be seen that a pH gradient (Calimet and Ullmann 2004) and a membrane potential (Bombarda et al. 2006) across the membrane influences in a non-trivial manner the protonation probabilities of some titratable residues which are known to participate in the proton transfer. The residues connected to one side of the membrane are influenced by the pH on the other side because of their electrostatic interactions with other titratable residues inside the protein. In bacteriorhodopsin, each site is uniquely connected through a hydrogen-bond network to either the cytoplasm or the extracellular space, as it is expected in proteins that perform vectorial pumping. Particularly interesting is the titration behavior of the residues Asp85 and Asp115, which are connected to the extracellular and the cytoplasmic side, respectively (Bombarda et al. 2006). Asp85 is the primary proton acceptor in the proton pumping cycle of bacteriorhodopsin. Therefore, it is crucial for the pumping cycle that Asp85 is deprotonated in the ground state of bacteriorhodopsin. The electrostatic interaction between Asp85 and Asp115 together with the interplay of their protonation states provide the structural basis for the regulation of proton pumping activity of bacteriorhodopsin. This interplay led to the proposal that the highly conserved Asp115 is involved in the regulation of the proton pumping activity. It was found experimentally that Asp115 is always protonated under conditions where no membrane potential

or no pH gradient is present (Haupts et al. 1999; Lanyi 2004; Garczarek and Gerwert 2006). From the electrostatic calculations, it can be seen that the protonation of this residue depends strongly on the pH gradient and the membrane potential. A very negative membrane potential or a high pH in the cell leads to the deprotonation of Asp115. The negatively charged Asp115 interacts strongly with Asp85 causing its protonation. A protonated Asp85 cannot accept a proton from the retinal Schiff base, and thus the proton pumping activity of bacteriorhodopsin is inhibited (Fig. 9b, c).

These electrostatic calculations on bacteriorhodopsin give an example how membrane proteins can sense the membrane potential and the pH gradient, and how the proton pumping can be regulated by these parameters. The method outlined here represents an useful tool to analyze the function of membrane proteins in their environment where membrane potential and concentration gradients are physiologically relevant.

Kinetics of charge transfer processes

To understand biochemical reactions, it is of crucial importance to study their reaction kinetics. The kinetics of charge transfer reactions can be simulated by a master equation approach. The rate constants which are required for such simulations can be calculated using electrostatic methods (Sham et al. 1999; Ferreira and Bashford 2006; Becker et al. 2007). Thus, combined with a master equation approach, continuum electrostatics also offers a possibility to access the non-equilibrium behavior of biomolecular systems.

Simulating chemical reactions using a master equation approach

In the microstate formalism given by Eqs. 6–9, charge transfer events are described as transitions between well-defined microstates of a system. The time dependence of the population of each microstate can be simulated using a master equation

$$\frac{\mathrm{d}}{\mathrm{d}t}P_\nu(t) = \sum_{\mu=1}^{M} k_{\nu\mu}P_\mu(t) - \sum_{\mu=1}^{M} k_{\mu\nu}P_\nu(t) \tag{17}$$

where $P_\nu(t)$ denotes the probability that the system is in charge state ν at time t, $k_{\nu\mu}$ denotes the probability per unit time that the system will change its state from μ to ν. The summation runs over all possible states μ. In order to restrict the number of states and only consider states that are accessible in a certain energy range, methods like extended Dead End Elimination (Kloppmann et al. 2007) can be used. Simulating charge transfer by Eq. 17 assumes that these processes can be described as a Markovian stochastic process. This assumption implies that the probability of a given charge transfer only depends on the current state of the system and not on the way in which the system has reached this state. This assumption is normally satisfied in biological electron transfer systems.

The system given by Eq. 17 is a system of coupled linear differential equations with constant coefficients, for which an analytical solution exists. Equation 17 describes the time evolution of the probability distribution of microstates of the system. For these microstates, energies G_ν and transition probabilities $k_{\nu\mu}$ can be assigned unambiguously. The time-dependent probability of finding a single site in the oxidized form can be obtained by summing up individual contributions from the time-dependent probabilities $P_\nu(t)$.

$$\langle x_i \rangle(t) = \sum_{\nu}^{M} x_{\nu,i}P_\nu(t) \tag{18}$$

Reaction rates

The outlined theory is directly applicable to a large class of reaction systems such as for example proton and electron transfer proteins. The determination of the rate constants $k_{\nu\mu}$ will, however, be specific for the particular reactions that should be simulated. For electron transfer systems, continuum electrostatic calculations in combination with existing empirical rate laws (Moser et al. 1992; Page et al. 1999) can be used to obtain electron transfer rates in good agreement with experimental data. Three factors mainly govern the rate constants of biological electron transfer reactions: the energy difference between the donor state and the acceptor state, the environmental polarization (reorganization energy), and the electronic coupling between the redox sites. The energy barrier for the transfer process is given in the framework of Marcus theory as

$$\Delta G^{\neq} = \frac{(\Delta G^\circ + \lambda)^2}{4\lambda} \tag{19}$$

where ΔG° is the energy difference between the donor state and the acceptor state and λ is the so-called reorganization energy. The electronic coupling between the redox sites is commonly accounted for by a distance-dependent exponential function $A\exp(-\beta(R-R_o))$ where R is the edge-to-edge distance between cofactors; R_o represents a van der Waals contact distance; and A represents an optimal rate. These aspects of biological electron transfer have been successfully combined to formulate a heuristic rate law applicable to long-range electron transfer (Moser et al. 1992; Page et al. 1999):

$$\log(k_{ex}) = 13 - 0.6\,(R - 3.6) - 3.1\,\frac{(\Delta G^\circ + \lambda)^2}{\lambda}$$
$$\log(k_{en}) = 13 - 0.6\,(R - 3.6) - 3.1\,\frac{(\Delta G^\circ + \lambda)^2}{\lambda} - \frac{\Delta G^\circ}{0.06} \quad (20)$$

where k_{ex} and k_{en} are the rate constants for exothermic and endothermic electron transfer reactions, respectively.

The free energy ΔG° for a transition between two states ν and μ can be calculated within the electrostatic model using Eq. 6. The reorganization energy λ contains two contributions, $\lambda = \lambda_o + \lambda_i$, where λ_o is the solvent reorganization energy and λ_i is the inner sphere reorganization energy. λ_o was shown to be accessible to calculations using electrostatic potentials obtained from the solution of the Poisson–Boltzmann equation (Marcus 1963; Sharp 1998):

$$\lambda_o = \frac{1}{2}\sum_i^K \left(\phi_{ad}^{opt}(\vec{r}_i) - \phi_{ad}(\vec{r}_i)\right)\Delta q_i^{ad} \quad (21)$$

where Δq_i^{ad} is the change in the charge of atom i when going from the donor state to the acceptor state. The potentials ϕ_{ad}^{opt} and ϕ_{ad} are generated by the charge distribution $\Delta\rho = \rho_a - \rho_d$ in a low (opt) and a high dielectric environment, respectively. Here, ρ_a and ρ_d denote the charge distribution of the acceptor state and the donor state, respectively. The low permittivity constant reflects the electronic polarizability (fast relaxation) while the high permittivity constant accounts also for the orientational polarizability (slow relaxation). The solvent reorganization energy is given by the difference in solvation free energy of the charge distribution $\Delta\rho$ between a low and a high dielectric environment. The inner sphere reorganization energy λ_i can be estimated by quantum chemical calculations and it is often found to be significantly smaller than the solvent reorganization energy (Marcus and Sutin 1985; Williams 1999; Olsson et al. 1998; Ryde and Olsson 2001). It is given by

$$\lambda_i = E_{bond}(\vec{r}_d, \rho_a) - E_{bond}(\vec{r}_a, \rho_a) \quad (22)$$

where E_{bond} is the total quantum chemical energy of the two sites; $\vec{r}_d$ and $\vec{r}_a$ correspond to the optimized geometry of the sites in the donor and acceptor state, respectively. Hence, the inner sphere reorganization energy is given by the difference in bonding energy between donor and acceptor geometry while the sites are kept in their acceptor state charge distribution (Olsson et al. 1998; Ryde and Olsson 2001).

Electron transfer from the C-subunit of the photosynthetic reaction center to the special pair

The approach described has been used to simulate the kinetics of electron transfer between the tetraheme-subunit and the special pair of the photosynthetic reaction center of *Blastochloris viridis* (Fig. 7a; Becker et al. 2007). The comparison with the experimental data (Ortega and Mathis 1993) shows that continuum electrostatic calculations can be used in combination with the empirical rate law of Eq. 20 to reproduce measurements on the rereduction kinetics of the photo-oxidized special pair (SP).

Rereduction of the SP in *B. viridis* is facilitated by the so-called C-subunit. The C-subunit contains four heme cofactors forming a transfer chain along the membrane normal. Electrons enter the C-subunit via a diffusing electron transport protein, which probably binds close to the outermost heme group (Ortega et al. 1999). The heme groups are commonly labeled according to their absorption maxima as c_{559}, c_{552}, c_{556}, and c_{554}. To simulate electron transfer within the C-subunit and between the C-subunit and the SP, a model was constructed consisting of the five redox-active groups. Redox potentials of these groups and interaction energies for pairs of these groups were calculated using the model with pure electrostatic interaction. In addition, the available structural information was used to calculate reorganization energies for all different pairs of redox-active groups.

In the experimental studies, Ortega et al. exposed the reaction center of *B. viridis* to different redox-potentials. The system was prepared in charge configurations with 4, 3, and 2 electrons distributed over the system consisting of the four hemes and the SP. The rereduction kinetics of the SP was measured after photo-induced oxidation. These experimental setups can be mimicked by simulations. To illustrate the kinetics seen in such simulations, the result obtained for a system starting from three electrons distributed over the four heme groups is described. On the left side of Fig. 10, the time-dependent probability distribution of the accessible microstates is shown. The corresponding oxidation probabilities for the hemes and the SP are shown on the right side. It can be seen that only a limited number of microstates contribute significantly to the probability distribution in the pico- to microsecond timescale. However, this feature does not imply that only this limited number of microstates is important for the kinetics of the system. The detailed information available from the simulation data allows to follow electron fluxes between microstates and thus electron movements between individual sites in a reaction scheme (Fig. 11).

The redox microstates can be denoted as vectors of 1 (reduced) and 0 (oxidized). The first element denotes the redox state of the special pair, the next four elements denote redox states of the hemes in the order of their distance to the SP, starting from the nearest. The kinetics depicted in Fig. 10 suggests a rather simple picture for the time dependence of the population of accessible microstates. Starting from a population of the two microstates (0, 1, 1, 1, 0) (90%) and (0, 1, 0, 1, 1) (10%) the system relaxes

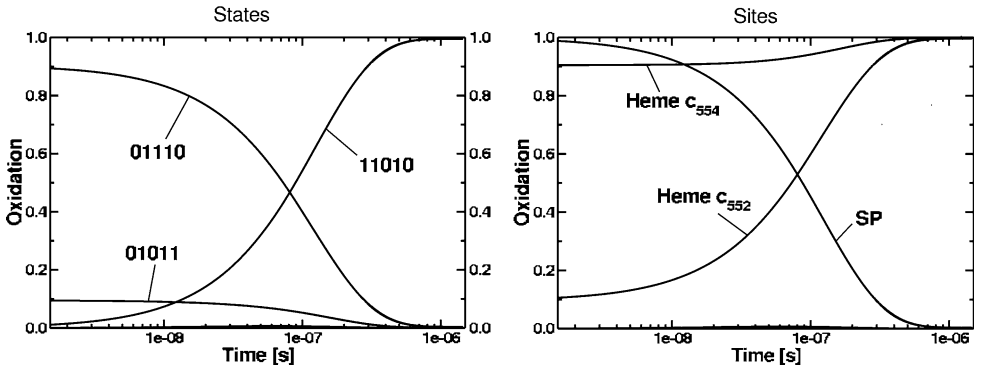

Fig. 10 Simulation of the rereduction kinetics of the special pair of the photosynthetic reaction center in a system with three electrons. The left picture depicts the time-dependent probability distribution of microstates after photo-oxidation of the SP simulated by Eq. 17. The state vector is given in the order (SP, c_{559}, c_{552}, c_{556}, c_{554}). In the state vector, 1 denotes a reduced site and 0 an oxidized site. The related oxidation probabilities of the four hemes and the SP is depicted in the right picture. Initially, three electrons are distributed among the four hemes. Initial distributions for the microstates were taken from an equilibrium distribution prior to photo-oxidation of the SP. States not shown are not significantly populated

toward an equilibrium distribution which is mainly given by one microstate (1,1,0,1,0). The underlying transfer dynamics of the system as depicted in Fig. 11, however, is considerably more complex. The highly populated initial state (0, 1, 1, 1, 0) can rapidly decay into the final state via just one intermediate (1, 0, 1, 1, 0). In contrast, the initial state (0, 1, 0, 1, 1) has to relax toward the final state via a succession of several intermediates. These intermediate states are only transiently populated. Each flux into one of these intermediates is accompanied by an equally high flux out of these intermediates. For example, the transition from the initial state (01011) to the intermediate (1,0,0,1,1) is rapidly followed by a transition to a second intermediate state (1,0,1,0,1). This intermediate state in turn either decays into state (1,0,1,1,0) via an electron transfer from heme c_{554} to heme c_{556} or alternatively to state (1,1,0,0,1) via electron transfer from heme c_{552} to heme c_{559}. As can be seen from the arrow in Fig. 11, electron transfer between two given sites is represented by more than one interstate transition. This multiplicity is a main obstacle in defining rate constants for transfer reactions between two given sites. However, the presented microstate formalism naturally incorporates this multiplicity and thus avoids the common ambiguities.

The procedure can be also applied to proton transfer reactions. Thus, the strategy to combine continuum electrostatics with the master equation represents an important method to understand the mechanism of complex charge transfer systems.

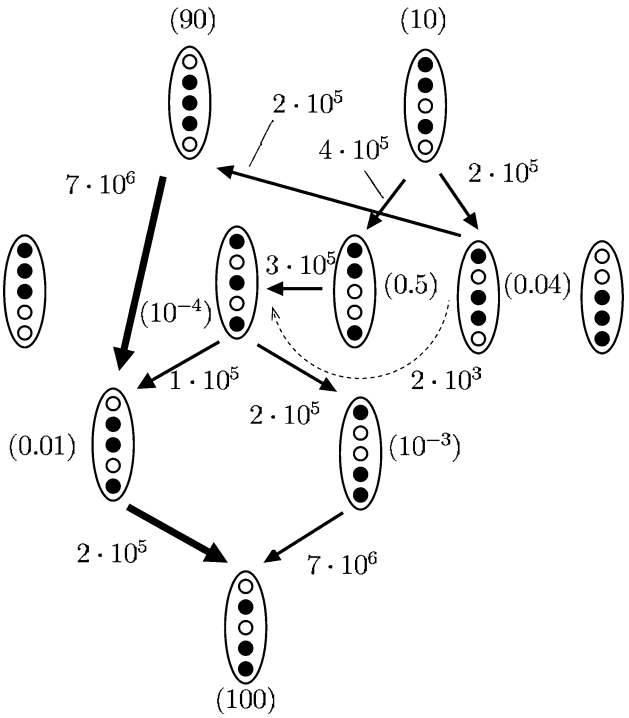

Fig. 11 Reaction scheme for the rereduction kinetics of the special pair of the photosynthetic reaction center in a system with three electrons. The reaction scheme is deduced from the flux analysis of the simulations in Fig. 10. Each oval represents a microstate of the system. The circles symbolize the redox cofactors in the order top to bottom: heme c_{554}, heme c_{556}, heme c_{552}, heme c_{559} and SP. Filled and open circles denote the reduced and oxidized form of the sites, respectively. The microstates representing the starting and the final configurations of the system in the simulation are depicted by the top and the bottom row, respectively. In the remaining middle rows, the intermediate microstates of the system are represented. For the starting and final microstates the respectively starting and final probability (in %) is given in parenthesis. For intermediate states, the values in parentheses denote the maximal probability observed during the simulation. Only fluxes (in s^{-1}) contributing significantly are indicated by arrows and their maximum value is given

Conclusions

The continuum electrostatic model based on the Poisson–Boltzmann equation provides a powerful tool in theoretical

biochemistry, because electrostatic interactions often play a major role in biological function. Conceptionally, this model describes the protein as a dielectric continuum of low permittivity with fixed point charges embedded in an environment with a high permittivity representing the solvent. The ions dissolved in the aqueous solution are represented as a charge density which adopts a Boltzmann distribution in the continuum with the high permittivity. The usefulness of this continuum electrostatic model goes far beyond the simple visual inspection of the electrostatic potentials. The Poisson–Boltzmann equation offers a mean to calculate electrostatic potentials and thus also electrostatic energies on the basis of the three dimensional structure of the protein. Applications of continuum electrostatics cover a wide range of subjects of central importance in photosynthesis research such as for instance protein docking, the coupling of proton, and electron transfer probabilities, and the analysis of the effect of membrane potentials. In combination with statistical thermodynamics, continuum electrostatics offers the possibility to calculate thermodynamic properties of proteins that can be directly compared to experimental measurements. The energetic parameters that can be calculated using the Poisson–Boltzmann equation can be used also for simulating kinetic processes using a master equation approach. As the examples provided in this article demonstrate, continuum electrostatic calculations allow to analyze biomolecules in atomic detail and to address specific mechanistic questions on the function of photosynthetic proteins.

Acknowledgments This work was supported by the Deutsche Forschungsgemeinschaft (UL 174/4, UL 174/6, UL 174/7). A. R. K. thanks the Boehringer Ingelheim Fonds for a doctoral fellowship. E. B. is supported by a postdoctoral Marie Curie fellowship (MCF 023403).

References

Abresch EC, Paddock ML, Stowell MHB, McPhillips TM, Axelrod HL, Soltis SM, Okamura MY, Feher G (1998) Identification of proton transfer pathways in the X-ray crystal structure of the bacterial reaction center from *Rhodobacter sphaeroides*. Photosynth Res 55:119–125

Ädelroth P, Paddock ML, Tehrani A, Beatty JT, Feher G, Okamura M (2001) Identification of the proton pathway in bacterial reaction centers: decrease of proton transfer rate by mutation of surface histidines at H126 and H128 and chemical rescue by imidazole identifies the initial proton donors. Biochemistry 40:14538–14546

Adolphs J, Renger T (2006) How proteins trigger excitation energy transfer in the FMO complex of green sulfur bacteria. Biophys J 91:2778

Alexov EG, Gunner MR (1999) Calculated protein and proton motions coupled to electron transfer: electron transfer from Q_A^- to Q_B in bacterial photosynthetic reaction centers. Biochemistry 38:8253–8270

Alexov E, Miksovska J, Baciou L, Schiffer M, Hanson DK, Sebban P, Gunner MR (2000) Modeling the effects of mutations on the free energy of the first electron transfer from Q_A^- to Q_B in photosynthetic reaction centers. Biochemistry 39:5940–5952

Andrew SM, Thomasson KA, Northrup SH (1993) Simulation of electron-transfer self-exchange in cytochromes *c* and b_5. J Am Chem Soc 115:5516–5521

Baciou L, Michel H (1995) Interruption of the water chain in the reaction center of *Rhodobacter sphaeroides* reduces the rates of the proton uptake and of the second electron transfer to Q_B. Biochemistry 34:7967–7972

Baker NA, Sept D, Joseph S, Holst MJ, McCammon JA (2001) Electrostatics of nanosystems: application to microtubules and the ribosome. Proc Natl Acad Sci USA 98:10037–10041

Baselt DR, Fodor S, van der Steen R, Lugtenburg J, Bogomolni RA, Mathies RA (1989) Halorhodopsin and sensory rhodopsin contain a C6-C7 s-*trans* retinal chromophore. Biophys J 55:193–196

Bashford D (1997) An object-oriented programming suite for electrostatic effects in biological molecules. In: Ishikawa Y, Oldehoeft RR, Reynders JVW, Tholburn M (eds) Scientific computing in object-oriented parallel environments. Springer, pp 233–240

Bashford D, Karplus M (1990) pK_as of ionizable groups in proteins: atomic detail from a continuum electrostatic model. Biochemistry 29:10219–10225

Bashford D, Gerwert K (1992) Electrostatic calculations of the pK_a values of ionizable groups in bacteriorhodopsin. J Mol Biol 224:473–486

Becker T, Ullmann RT, Ullmann GM (2007) Simulation of the electron transfer between the tetraheme-subunit and the special pair of the photosynthetic reaction center using a microstate description. J Phys Chem B 111:2957–2968

Belrhali H, Nollert P, Royant A, Menzel C, Rosenbusch JP, Landau EM, Pebay-Peyroula E (1999) Protein, lipid and water organization in bacteriorhodopsin crystals: a molecular view of the purple membrane at 1.9 Å resolution. Structure 7:909–917

Beratan DN, Onuchic JN (1989) Electron-tunneling pathways in ruthenated proteins: influences on transfer rate. Photosynth Res 22:173–186

Beratan DN, Onuchic JN, Hopfield JJ (1985) Limiting forms of the tunneling matrix element in the long distance bridged electron transfer problem. J Chem Phys 83:5325–5329

Beratan DN, Onuchic JN, Betts JN, Bowler BE, Gray HB (1990) Electron-tunneling pathways in ruthenated proteins. J Am Chem Soc 112:7915–7921

Beratan DN, Betts JN, Onuchic JN (1991) Protein electron transfer rates set by the briding secondary and tertiary structure. Science 252:1285–1288

Beroza P, Fredkin DR, Okamura MY, Feher G (1991) Protonation of interacting residues in a protein by a Monte Carlo method: application to lysozyme and the photosynthetic reaction center. Proc Natl Acad Sci USA 88:5804–5808

Betts JN, Beratan DN, Onuchic JN (1992) Mapping electron tunneling pathways: an algorithm that finds the "minimum length"/maximum coupling pathway between electron donors and acceptors in proteins. J Am Chem Soc 114:4043–4046

Bombarda E, Becker T, Ullmann GM (2006) The influence of the membrane potential on the protonation of bacteriorhodopsin: insights from electrostatic calculations into the regulation of proton pumping. J Am Chem Soc 128:12129–12139

Borodich A, Ullmann GM (2004) Internal hydration of protein cavities: studies on BPTI. PCCP 6:1906–1911

Brooks BR, Bruccoleri RE, Olafson BD, States DJ, Swaminathan S, Karplus M (1983) CHARMM: a program for macromolecular

energy, minimization, and dynamics calculation. J Comput Chem 4:187–217

Calimet N, Ullmann GM (2004). The influence of a transmembrane pH gradient on protonation probabilities of bacteriorhodopsin: the structural basis of the back-pressure effect. J Mol Biol 339:571–589

Cogdell RJ, Gall A, Köhler J (2006) The architecture and function of the light-harvesting apparatus of purple bacteria: from single molecules to in vivo membranes. Q Rev Biophys 39:227–292

Colbert CL, Couture MM-J, Eltis LD, Bolin JT (2000) A cluster exposed: structure of the Rieske ferredoxin from biphenyl dioxygenase and the redox properties of Rieske Fe–S proteins. Structure 8:1267–1278

Crnogorac M, Ullmann GM, Kostić NM (2001) Effects of pH on protein association. Modification of the proton linkage model and experimental verification of the modified model in the case of cytochrome c and plastocyanin. J Am Chem Soc 123:10789–10798

Daune M (1999) Molecular biophysics. University Press, Oxford

De Rienzo F, Gabdoulline RRM, Cristina Menziani PGDB, Wade RC (2001) Electrostatic analysis and Brownian dynamics simulation of the association of plastocyanin and cytochrome f. Biophys J 81:3090–3104

Denke E, Merbitz-Zahradnik T, Hatzfeld OM, Snyder CH, Link TA, Trumpower BL (1998) Alteration of the midpoint potential and catalytic activity of the Rieske iron-sulfur protein by changes of amino acids forming hydrogen bonds to the iron-sulfur cluster. J Biol Chem 273(15):9085–9093

Ferreira A, Bashford D (2006) Model for proton transport coupled to protein conformational change: application to proton pumping in the bacteriorhodopsin photocycle. J Am Chem Soc 128: 16778–16790

Friesner RA, Beachy MD (1998) Quantum mechanical calculations on biological systems. Curr Opin Struct Biol 8:257–262

Gabdoulline RR, Wade RC (2002) Biomolecular diffusional association. Curr Opin Struct Biol 12:204–213

Garczarek F, Gerwert K (2006) Polarized FTIR spectroscopy in conjunction with in situ H/D exchange reveals the orientation of protein internal carboxylic acids. J Am Chem Soc 128:28–29

Graige MS, Paddock ML, Bruce JM, Feher G, Okamura MY (1996) Mechanism of proton-coupled electron transfer for quinone (Q_B) reduction in reaction centers of *Rb. sphaeroides*. J Am Chem Soc 118:9005–9016

Gross EL, Rosenberg I (2006) A brownian dynamics study of the interaction of Phormidium cytochrome f with various cyanobacterial plastocyanins. Biophys J 90:366–380

Gunner M, Alexov E (2000) A pragmatic approach to structure based calculation of coupled proton and electron transfer in proteins. Biochim Biophys Acta 1458:63–87

Gunner MR, Mao J, Song Y, Kim J (2006) Factors influencing the energetics of electron and proton transfers in proteins. What can be learned from calculations. Biochim Biophys Acta 1757: 942–968

Haddadian EJ, Gross EL (2005) Brownian dynamics study of cytochrome f interactions with cytochrome c(6) and plastocyanin in *Chlamydomonas reinhardtii* plastocyanin, and cytochrome c(6) mutants. Biophys J 88:2323–2339

Haddadian EJ, Gross EL (2006) A Brownian dynamics study of the effects of cytochrome *f* structure and deletion of its small domain in interactions with cytochrome c_6 and plastocyanin in *Chlamydomonas reinhardtii*. Biophys J 90:566–577

Harbison GS, Smith SO, Pardoen JA, Courtin JML, Lugtenburg J, Herzfeld J, Mathies RA, Griffin RG (1985) Solid-state 13C NMR detection of a perturbed 6-s-*trans chromophore in bacteriorhodopsin*. Biochemistry 24:6955–6962

Haupts U, Tittor J, Oesterhelt D (1999) Closing in on bacteriorhodopsin: progress in understanding the molecule. Annu Rev Biophys Struct Biol 28:367–399

Hayashi S, Tajkhorshid E, Pebay-Peyroula E, Royant A, Landau EM, Navarro J, Schulten K (2001) Structural determinants of spectral tuning in retinal proteins—bacteriorhodopsin vs. sensory rhodopsin II. J Phys Chem B 105:10124–10131

Hervás M, Navarro JA, De La Rosa MA (2003) Electron transfer between membrane complexes and soluble proteins in photosynthesis. Acc Chem Res 36:798–805

Hienerwadel R, Grzybek S, Fogel C, Kreutz W, Okamura MY, Paddock ML, Breton J, Nabedryk E, Mäntele W (1995) Protonation of Glu L212 following Q^-_B formation in the photosynthetic reaction center of *Rhodobacter sphaeroides*: evidence from time-resolved infrared spectroscopy. Biochemistry 34:2832–2843

Hill TL (1960) An introduction to statistical thermodynamics. Dover Publ, Inc., New York

Hodgkin E, Richards W (1987) Molecular similarity based on electrostatic potential and electric field. Int J Quant Chem Quant Biol Symp 14:105–110

Honig B, Nicholls A (1995) Classical electrostatics in biology and chemistry. Science 268:1144–1149

Hu X, Ritz T, Damjanovic A, Autenrieth F, Schulten K (2002) Photosynthetic apparatus of purple bacteria. Q Rev Biophys 35:1–62

Im W, Beglov D, Roux B (1998) Continuum solvation model: electrostatic forces from numerical solutions to the Poisson–Boltzmann equation. Comput Phys Commun 111:59–75

Ishikita H, Knapp E-W (2004) Variation of Ser-L223 hydrogen bonding with the Q_B redox state in reaction centers from *Rhodobacter sphaeroides*. J Am Chem Soc 126:8059–8064

Ishiktia H, Knapp EW (2005) Energetics of proton transfer pathways in reaction centers from *Rhodobacter sphaeroides*. J Biol Chem 280:12446–12450

Ivković-Jensen MM, Ullmann GM, Young S, Hansson Ö, Crnogorac M, Edjebäck M, Kostić NM (1998) Effects of single and double mutations in plastocyanin on the rate constant and activation parameters of the gated electron-transfer reaction between the triplet state of zinc cytochrome *c* and cupriplastocyanin. Biochemistry 37:9557–9569

Ivković-Jensen MM, Ullmann GM, Crnogorac MM, Ejdebäck M, Young S, Hansson Ö, Kostić NM (1999) Comparing the rates and the activation parameters for the forward reaction between the triplet state of zinc cytochrome c and cupriplastocyanin and the back reaction between the zinc cytochrome c cation radical and cuproplastocyanin. Biochemistry 38:1589–1597

Jensen F (1999) Introduction to computational chemistry. Wiley, Chichester

Kandori H, Shimono K, Sudo Y, Iwamoto M, Shichida Y, Kamo N (2001) Structural changes of *Pharaonis* phoborhodopsin upon photoisomerization of the retinal chromophore: infrared spectral comparison with bacteriorhodopsin. Biochemistry 40:9238–9246

Klingen AR, Ullmann GM (2004) Negatively charged residues and hydrogen bonds tune the ligand histidine pK_a values of Rieske iron-sulfur proteins. Biochemistry 43(39):12383–12389

Klingen AR, Ullmann GM (2006) Theoretical investigation of the behavior of titratable groups in proteins. Photochem Photobiol Sci 5:588–596

Klingen AR, Palsdottir H, Hunte C, Ullmann GM (2007) Continuum electrostatic calculations of redox-dependent protonation state changes in cytochrome bc_1. Biochim Biophys Acta 1767:204–221

Kloppmann E, Becker T, Ullmann GM (2005) Electrostatic potential at the retinal of three archaeal rhodopsins: implications for their different absorption spectra. Proteins 61:953–965

Kloppmann E, Ullmann GM, Becker T (2007). An extended dead-end elimination algorithm to determine gap-free lists of low energy states. J Comput Chem 28:2325–2335

Koepke J, Krammer E-M, Klingen AR, Sebban P, Ullmann GM, Fritzsch G (2007) pH modulates the quinone position in the photosynthetic reaction center from *Rhodobacter sphaeroides* in the neutral and charge separated states. J Mol Biol 371:396–409

Kostić NM (1996) Dynamic aspects of electron-transfer reactions in metalloprotein complexes. In: Pittman CU (ed) Metal-containing polymeric materials. Plenum Press, New York, pp 491–500

Lanyi JK (2004) Bacteriorhodopsin. Annu Rev Physiol 2004:665–688

Leach AR (1996) Molecular modelling: principles and applications. Addison, Wesley, Longman, Essex UK

Leggate EJ, Bill E, Essigke T, Ullmann GM, Hirst J (2004) Formation and characterization of an all-ferrous Rieske cluster, and stabilization of the $[2Fe\text{-}2S]^0$ core by protonation. Proc Natl Acad Sci USA 101:10913–10918

Li J, Fischer CL, Chen JL, Bashford D, Noodleman L (1996) Calculation of redox potentials and pK_a values of hydrated transition metal cations by a combined density functional and continuum dielectric theory. J Phys Chem 96:2855–2866

Li J, Nelson MR, Peng CY, Bashford D, Noodleman L (1998) Incorporating protein environments in density functional theory: a self-consistent reaction field calculation of redox potentials of [2Fe2S] clusters in ferredoxin and phthalate dioxygenase reductase. J Phys Chem A 102:6311–6324

Lin IJ, Chen Y, Fee JA, Song J, Westler WM, Markley JL (2006) Rieske protein from *Thermus thermophilus*: (15)N NMR titration study demonstrates the role of iron-ligated histidines in the pH dependence of the reduction potential. J Am Chem Soc 128:10672–10673

Link TA (1994) Two pK values of the oxidized Rieske [2Fe-2S] cluster observed by CD spectroscopy. Biochim Biophys Acta 1185:81–84

Liu T, Han W-G, Himo F, Ullmann GM, Bashford D, Toutchkine A, Hahn KM, Noodleman L (2004) Density functional vertical self-consistent reaction field theory for solvatochromism studies of solvent-sensitive dyes. J Phys Chem B 108:11157–11169

Luecke H, Schobert B, Richter H-T, Cartailler J-P, Lanyi JK (1999) Structure of bacteriorhodopsin at 1.55 Å resolution. J Mol Biol 291:899–911

Luecke H, Schobert B, Lanyi JK, Spudich EN, Spudich JL (2001) Crystal structure of sensory rhodopsin II at 2.4 angstroms: insights into color tuning and transducer interaction. Science 293:1499–1502

Luo R, David L, Gilson MK (2002) Accelerated Poisson–Boltzmann calculations for static and dynamic systems. J Comput Chem 23:1244–1253

Madjet ME, Abdurahman A, Renger T (2006) Interpigment Coulomb couplings from ab-initio transition charges: application to strongly coupled pigments in photosynthetic antennae and reaction centers. J Phys Chem B 110:17268

Madura JD, Davis ME, Gilson MK, Wade RC, Luty BA, McCammon JA (1994) Biological applications of electrostatic calculations and Brownian dynamics. Rev Comput Chem 5:229–267

Marcus RA (1963) Free energy of nonequilibrium polarization systems. II. Homogeneous and electrode systems. J Chem Phys 38:1858–1862

Marcus RA, Sutin N (1985) Electron transfer in chemistry and biology. Biochim Biophys Acta 811:265–322

Metropolis N, Rosenbluth AW, Rosenbluth MN, Teller AH (1953) Equation of state calculation by fast computing machines. J Chem Phys 21:1087–1092

Miksovska J, Kálmán L, Schiffer M, Maróti PDK, Hanson PS (1997) In bacterial reaction centers rapid delivery of the second proton to Q_B can be achieved in the absence of L212Glu. Biochemistry 36:12216–12226

Moser CC, Keske JM, Warncke K, Farid RS, Dutton PL (1992) Nature of biological electron transfer. Nature 355:796–802

Nielsen JE, McCammon JA (2003) Calculating pKa values in enzyme active sites. Protein Sci 12:1894–1901

Northrup SH (1994) Hydrodynamic motions of large molecules. Curr Opin Struct Biol 4:269–274

Northrup SH, Allison SA, McCammon JA (1984) Brownian dynamics simulation of diffusion-influenced bimolecular reactions. J Chem Phys 80:1517–1524

Okamura MY, Paddock ML, Graige MS, Feher G (2000) Proton and electron transfer in bacterial reaction center. Biochim Biophys Acta 145:148–163

Olsson MHM, Ryde U, Roos BO (1998) Quantum chemical calculation of the reorganization energy of blue copper proteins. Protein Sci 81:6554–6558

Onufriev A, Ullmann GM (2004) Decomposing complex ligand binding into simple components: connections between microscopic and macroscopic models. J Phys Chem B 108:11157–11169

Onufriev A, Case DA, Ullmann GM (2001) A novel view on the pH titration of biomolecules. Biochemistry 40:3413–3419

Onufriev A, Smondyrev A, Bashford D (2003) Proton affinity changes driving unidirectional proton transport in the bacteriorhodopsin photocycle. J Mol Biol 332:1183–1193

Ortega JM, Mathis P (1993) Electron transfer from the tetraheme cytochrome to the special pair in isolated reaction centers of *Rhodopseudomonas viridis*. Biochemistry 32:1141–1151

Ortega JM, Drepper F, Mathis P (1999) Electron transfer between cytochrome c_2 and the tetraheme cytochrome in *Rhodopseudomonas viridis*. Photosynth Res 59:147–157

Paddock ML, Rongley SH, Feher G, Okamura MY (1989) Pathway of proton transfer in bacterial reaction centers: replacement of glutamic acid 212 in the L subunit by glutamine inhibits quinone (secondary acceptor) turnover. Proc Natl Acad Sci USA 86:6602–6606

Paddock ML, McPherson PH, Feher G, Okamura MY (1990) Pathway of proton transfer in bacterial reaction centers: replacement of serine-L223 by alanine inhibits electron and proton transfers associated with reduction of quinone to dihydroquinone. Proc Natl Acad Sci USA 87:6803–6807

Paddock ML, Rongey SH, McPherson PH, Juth A, Feher G, Yokamura M (1994) Pathway of proton transfer in bacterial reaction centers: role of Aspartate-L213 in proton transfers associated with reduction of quinone to dihydroquinone. Biochemistry 33:734–745

Paddock ML, Feher G, Okamura MY (1997) Proton and electron transfer to the secondary quinone (Q_B) in bacterial reaction centers: the effect of changing the electrostatics in the vicinity of Q_B by interchanging Asp and Glu at L212and L213 sites. Biochemistry 36:14238–14249

Paddock ML, Senft ME, Graige MS, Rongey SH, Turanchik T, Feher G, Okamura MY (1998) Characterization of second site mutations show that fast proton transfer to Q_B^- is restored in bacterial reaction centers of *Rhodobacter sphaeroides* containing the Asp-L213 → Asn lesion. Photosynth Res 58:281–291

Paddock ML, Ädelroth P, Chang C, Abresch EC, Feher G, Okamura MY (2001) Identification of the proton pathway in bacterial reaction centers: cooperation between Asp-M17 and Asp-L210 facilitates proton transfer to the secondary quinone (Q_B). Biochemistry 40:6893–6902

Paddock ML, Feher G, Okamura MY (2003) Proton transfer pathways and mechanism in bacterial reaction centers. FEBS Lett 555: 45–50

Page CC, Moser CC, Chen X, Dutton PL (1999) Natural engineering principles of electron tunneling in biological oxidation-reduction. Nature 402:47–52

Pearson DC, Gross EL (1995) The docking of cytochrome *f* with plastocyanin: three possible complexes. In: Mathis P (ed) Photosynthesis: from light to biosphere, vol II. Kluwer Academic Publishers, Dordrecht, The Netherlands, pp 729–732

Pearson DC, Gross EL, David E (1996) Electrostatic properties of cytochrome *f*: implications for docking with plastocyanin. Biophys J 71:64–76

Prabhu NV, Zhu P, Sharp KA (2004) Implementation and testing of stable, fast implicit solvation in molecular dynamics using the smooth-permittivity finite difference Poisson–Boltzmann method. J Comput Chem 25:2049–2064

Qin L, Kostić NM (1993) Importance of protein rearrangement in the electron-transfer reaction between the physiological partners cytochrome *f* and plastocyanin. Biochemistry 32:6073–6080

Rabenstein B, Ullmann GM (1998) Calculation of protonation patterns in proteins with structural relaxation and molecular ensembles—application to the photosynthetic reaction center. Eur Biophys J 27:626–637

Rabenstein B, Ullmann GM, Knapp EW (1998) Energetics of electron-transfer and protonation reactions of the quinones in the photosynthetic reaction center of *Rhodopseudomonas viridis*. Biochemistry 37:2488–2495

Rabenstein B, Ullmann GM, Knapp EW (2000) Electron transfer between the quinones in the photosynthetic reaction center and its coupling to conformational changes. Biochemistry 39:10496–10587

Reiss H, Heller A (1985) The absolute potential of the standard hydrogen electrode: a new estimate. J Phys Chem 89:4207–4213

Ren L, Martin CH, Wise KJ, Gillespie NB, Luecke H, Lanyi JK, Spudich JL, Birge RR (2001) Molecular mechanism of spectral tuning in sensory rhodopsin II. Biochemistry 40:13906–13914

Richards FM (1977) Areas, volumes, packing and protein structure. Annu Rev Biophys Bioeng 6:151–176

Ritz T, Damjanovic A, Schulten K (2002) The quantum physics of photosynthesis. ChemPhysChem 3:243–248

Roberts VA, Freeman HC, Olson AJ, Tainer JA, Getzoff ED (1991) Electrostatic orientation of the electron-transfer complex between plastocyanin and cytochrome *c*. J Biol Chem 266:13431–13441

Roux B (1997) The influence of the membrane potential on the free energy of an intrinsic protein. Biophys J 73:2981–2989

Royant A, Nollert P, Edman K, Neutze R, Landau EM, Pebay-Peyroula E (2001) X-ray structure of sensory rhodopsin II at 2.1-Å resolution. Proc Natl Acad Sci USA 98:10131–10136

Ryde U, Olsson MHM (2001) Structure, strain and reorganization energy of blue copper models in the protein. Int J Quant Chem 81:335–347

Sakamoto M, Wada A, Akai A, Ito M, Goshima T, Takahashi T (1998) Evidence for the archaebacterial-type conformation about the bond between the small β-ionone ring and the polyene chain of the chromophore retinal in chlamyrhodopsin. FEBS Lett 434:335–338

Sampogna RV, Honig B (1994) Environmental effects on the protonation states of active site residues in bacteriorhodopsin. Biophys J 66:1341–1352

Sampogna RV, Honig B (1996) Electrostatic coupling between retinal isomerization and the ionization state of Glu-204: a general mechanism for proton release in bacteriorhodopsin. Biophys J 71:1165–1171

Scharnagl C, Hettenkofer J, Fischer SF (1994) Proton release pathway in bacteriorhodopsin: molecular dynamics and electrostatic calculations. Int J Quant Chem 52:33–56

Sebban P, Maróti P, Hanson DK (1995) Electron and proton transfer to the quinones in bacterial photosynthetic reaction centers: insight from combined approaches of molecular genetics and biophysics. Biochimie 77:677–694

Sener M, Lu D, Park S, Damjanovic A, Ritz TPF, Schulten K (2004) Excitation migration in trimeric cyanobacterial photosystem I. J Chem Phys 120:11183–11195

Sengupta D, Behera RN, Smith JC, Ullmann GM (2005a) The α-helix dipole – Screened out? Structure 13:849–855

Sengupta D, Meinhold L, Langosch D, Ullmann GM, Smith JC (2005b) Energetics of helical-peptide orientations in membranes. Proteins 58:913–922

Senn HM, Thiel W (2007) QM/MM studies of enzymes. Curr Opin Chem Biol 11:182–187

Sham YY, Muegge I, Warshel A (1999) simulating proton translocations in proteins: probing proton transfer pathways in the *Rhodobacter sphaeroides* reaction center. Proteins 36:484–500

Sharp KE (1998) Calculation of electron transfer reorganization energies using the Finite Difference Poisson–Boltzmann model. Biophys J 73:1241–1250

Sokerina EV, Ullmann GM, van Pouderoyen G, Canters GW, Kostić NM (1999) Electrostatic effects on the kinetics of photoinduced electron-transfer reactions of the triplet state of zinc cytochrome c with wild-type and mutant forms of *Pseudomonas aeruginosa* azurin. J Biol Inorg Chem 4:111–121

Song Y, Mao J, Gunner MR (2003). Calculation of proton transfers in bacteriorhodopsin bR and M intermediates. Biochemistry 42:9875–9888

Spassov VZ, Luecke H, Gerwert K, Bashford D (2001) pK_a calculations suggest storage of an excess proton in a hydrogen-bonded water network in bacteriorhodopsin. J Mol Biol 312:203–219

Stowell MHV, McPhillips TM, Rees DC, Soltis SM, Abresch E, Feher G (1997) Light-induced structural changes in photosynthetic reaction center: implications for mechanism of electron-proton transfer. Science 276:812–816

Takahashi E, Wraight CA (1992) Proton and electron transfer in the acceptor quinone complex of *Rhodobacter sphaeroides* reaction centers: characterization of site-directed mutants of the two ionizable residues, Glu^{L212} and Asp^{L213}, in the Q_B binding site. Biochemistry 31:855–866

Taly A, Sebban P, Smith JC, Ullmann GM (2003) The position of Q_B in the photosynthetic reaction center depends on pH: a theoretical analysis of the proton uptake upon Q_B reduction. Biophys J 84:2090–2098

Ubbink M (2004) Complexes of photosynthetic redox proteins studied by NMR. Photosyn Res 81:277–287

Ubbink M, Ejdebäck M, Karlson BG, Bendall DS (1998) The structure of the complex of plastocyanin and cytochrome *f*, determined by paramagnetic NMR and restrained rigid body molecular dynamics. Structure 6:323–335

Ullmann GM (2000) The coupling of protonation and reduction in proteins with multiple redox centers: theory, computational method, and application to cytochrome c_3. J Phys Chem B 104:6293–6301

Ullmann GM (2003) Relations between protonation constants and titration curves in polyprotic acids: a critical view. J Phys Chem B 107:6293–6301

Ullmann GM, Kostić NM (1995) Electron-tunneling paths in various electrostatic complexes between cytochrome *c* and plastocyanin. Anisotropy of the copper-ligand interactions and dependence of the iron-copper electronic coupling on the metalloprotein orientation. J Am Chem Soc 117:4766–4774

Ullmann GM, Knapp EW (1999) Electrostatic computations of protonation and redox equilibria in proteins. Eur Biophys J 28:533–551

Ullmann GM, Hauswald M, Jensen A, Kostić NM, Knapp EW (1997a) Comparison of the physiologically-equivalent proteins cytochrome c_6 and plastocyanin on the basis of their electrostatic potentials. Tryptophane 63 in cytochrome c_6 may be isofunctional with Tyrosine 83 in plastocyanin. Biochemistry 36:16187–16196

Ullmann GM, Knapp EW, Kostić NM (1997b) Computational simulation and analysis of the dynamic association between plastocyanin and cytochrome *f*. Consequences for the electron-transfer reaction. J Am Chem Soc 119:42–52

Ullmann GM, Hauswald M, Jensen A, Knapp EW (2000) Superposition of ferredoxin and flavodoxin using their electrostatic potentials. Implications for their interactions with photosystem I and ferredoxin:NADP reductase. Proteins 38:301–309

Ullmann GM, Noodleman L, Case DA (2002) Density functional calculation of the pK_a values and redox potentials in the bovine Rieske iron-sulfur protein. J Biol Inorg Chem 7:632–639

van Gunsteren WF, Bakowies D, Baron R, Chandrasekhar I, Christen M, Daura X, Gee P, Geerke DP, Glattli A, Hunenberger PH, Kastenholz MA, Oostenbrink C, Schenk M, Trzesniak D, van der Vegt NFA, Yu HB (2001) Biomolecular modeling: goals, problems, perspectives. Angew Chem Int Ed Engl 45:4064–4092

Williams RJP (1999) Electron transfer and proton coupling in proteins. J Solid State Chem 145:488–495

Zhou JS, Kostić NM (1993) Gating of the photoinduced electron transfer from zinc cytochrome *c* and tin cytochrome *c* to plastocyanin. Effects of the solution viscosity on the rearrangement of the metalloproteins. J Am Chem Soc 115:10796–10804

Zu Y, Fee JA, Hirst J (2001) Complete thermodynamic characterization of reduction and protonation of the bc1-type Rieske [2Fe-2S] center of *Thermus thermophilus*. J Biol Chem 276:9906–9907